Scanning Electrochemical Microscopy

Shigeru Amemiya,[1] Allen J. Bard,[2] Fu-Ren F. Fan,[2] Michael V. Mirkin,[3] and Patrick R. Unwin[4]

[1]University of Pittsburgh, Department of Chemistry, Pittsburgh, Pennsylvania 15260
[2]University of Texas at Austin, Department of Chemistry and Biochemistry, Austin, Texas 78712; email: ajbard@mail.utexas.edu
[3]Queens College, Department of Chemistry and Biochemistry, Flushing, New York 11367
[4]University of Warwick, Department of Chemistry, Coventry CV4 7AL, United Kingdom

Annu. Rev. Anal. Chem. 2008. 1:95–131

First published online as a Review in Advance on December 20, 2007

The *Annual Review of Analytical Chemistry* is online at anchem.annualreviews.org

This article's doi:
10.1146/annurev.anchem.1.031207.112938

1936-1327/08/0719-0095$20.00

Key Words

ultramicroelectrode, charge transport, interface, scanning probe microscopy, electroanalytical chemistry

Abstract

This review describes work done in scanning electrochemical microscopy (SECM) since 2000 with an emphasis on new applications and important trends, such as nanometer-sized tips. SECM has been adapted to investigate charge transport across liquid/liquid interfaces and to probe charge transport in thin films and membranes. It has been used in biological systems like single cells to study ion transport in channels, as well as cellular and enzyme activity. It is also a powerful and useful tool for the evaluation of the electrocatalytic activities of different materials for useful reactions, such as oxygen reduction and hydrogen oxidation. SECM has also been used as an electrochemical tool for studies of the local properties and reactivity of a wide variety of materials, including metals, insulators, and semiconductors. Finally, SECM has been combined with several other nonelectrochemical techniques, such as atomic force microscopy, to enhance and complement the information available from SECM alone.

1. INTRODUCTION

Scanning electrochemical microscopy (SECM) employs an ultramicroelectrode (UME), also known as a tip, to scan in close proximity to a surface of interest. The electrochemical response of the tip (or of the substrate in response to the tip) provides quantitative information about the interfacial region. Since the technique was first reported in 1989, approximately 1000 papers have been published on its methodology and applications, and numerous reviews have appeared. The basics of the technique, the instrumentation, and many applications through about 2000 have been thoroughly covered in a monograph (1). This review mainly covers work that has been done since 2000 and emphasizes the new and important trends in SECM.

2. NANOMETER-SIZED TIPS AND THEIR APPLICATIONS

2.1. Overview

Nanometer-sized tips offer important advantages for various SECM applications. In kinetic experiments, nanoelectrodes offer high mass-transfer rates under steady-state conditions in combination with practically negligible effects of the resistive potential drop in solution, double layer charging current, and low levels of reactant adsorption. The high spatial resolution achievable with such tips makes nanoscale electrochemical imaging possible. The small size of the scanning probe is essential for subcellular-level studies of biological systems and single-molecule experiments.

2.2. Preparation and Characterization

A simple way to produce nm-sized conical tips is to etch a metal wire and then coat it with an insulator—e.g., molten Apiezon wax (2)—while leaving the apex exposed. Investigators have tried other types of coating, including varnish, molten paraffin, silica coating, poly(α-methylstyrene), polyimide (3), electropolymerized phenol, and electrophoretic paint (4). Sub-μm-sized conical carbon tips have been prepared using flame etching (5).

Disk-type tips can be prepared using a micropipette puller (6–8). Recently, it was shown that a tip as small as ~10-nm-radius can be polished on a lapping tape under video-microscopic control (8). The polished flat nanotips yield more reliable and reproducible data and can be used for fast kinetic measurements. Another type of nm-sized SECM probe—the slightly recessed nanotip—has also been prepared by etching polished Pt nanoelectrodes (9).

The shape and size of a nanotip can be characterized by a combination of voltammetry and SECM (6, 8–10). In **Figure 1**, an SECM approach curve (*a*) and a steady-state voltammogram (*b*) were obtained with the same polished Pt electrode. The experimental current versus distance curve in **Figure 1*a*** fits the theoretical curve calculated with $a = 46$ nm that was obtained from the limiting current in **Figure 1*b***. This radius value is reliable because of the high positive feedback current (up to a normalized current of 8) obtained in **Figure 1*a***. The distance of the closest

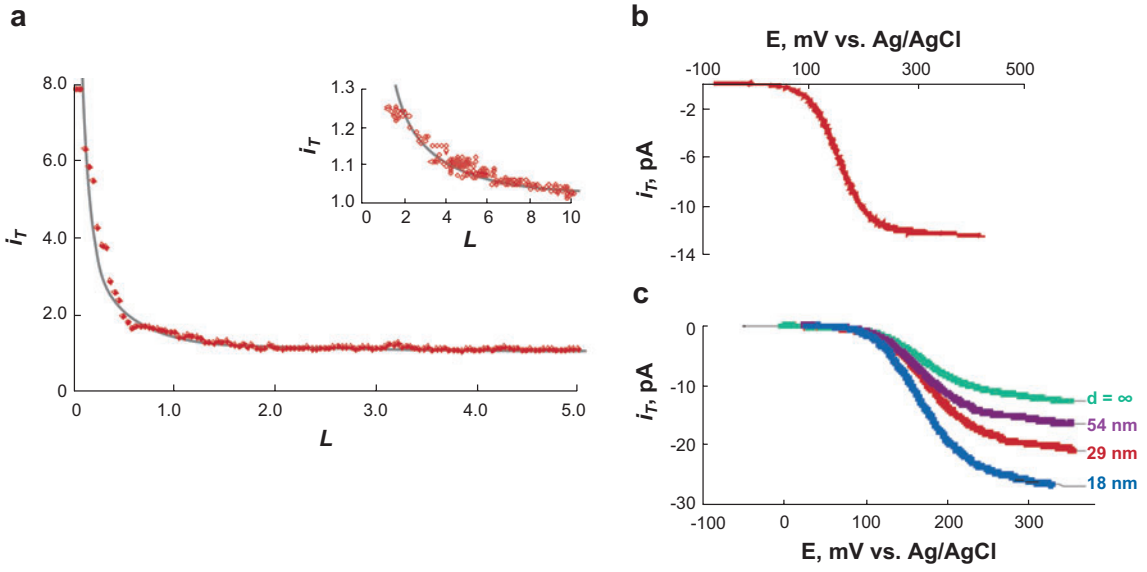

Figure 1

(*a*) Scanning electrochemical microscopy current versus distance curve; (*b*) steady-state voltammogram obtained in the bulk solution; and (*c*) four voltammograms for different tip/substrate separation distances. Aqueous solution contained 1 mM ferrocenemethanol and 0.2 M NaCl. (*a*) Solid line indicates theoretical approach curve for diffusion-controlled positive feedback; symbols represent experimental data. The tip approached the unbiased Au film substrate with a speed of 5 nm/s. The tip was either a 46-nm (panels *a* and *b*) or a 36-nm (panel c) polished Pt electrode. The inset in panel a shows an approach curve for a 13-nm tip. (*c*) Experimental (*symbols*) and theoretical (*solid lines*) voltammograms obtained at the tip-substrate distance, $d = \infty$ (*1*), 54 nm (*2*), 29 nm (*3*), and 18 nm (*4*). Adapted with permission from Reference 8. Copyright 2007, American Chemical Society.

approach in **Figure 1*a*** (~5 nm) could be achieved only with the essentially flat and well-polished tip surface.

2.3. Penetration Experiments

Nm-sized tips can be used to penetrate a microstructure (e.g., a sub-μm-thick polymer film containing fixed redox centers or loaded with a redox mediator) and can extract spatially resolved information about concentrations and kinetic and mass-transport parameters (11, 12). With a tip inside the film, relatively far from the underlying conductor or insulator, solid-state voltammetry at the tip can be carried out similarly to conventional voltammetric experiments in solution. At smaller distances, the tip current either increases or decreases depending on the rate of the mediator regeneration at the substrate. If the film is homogeneous and not very resistive, the current-distance curves are similar to those obtained in solution. In this way, kinetic parameters, diffusion coefficients, and formal potential for $Os(bpy)_3^{2+/3+}$ in Nafion were extracted from steady-state voltammograms at a nm-sized conical tip (11). For

poly(vinylferrocene), the depth profile of film resistance was obtained by scanning the tip across a 300-nm-thick layer (12).

2.4. Imaging

The attainable resolution in SECM depends upon the tip radius and separation distance between tip and sample. The use of nm-sized tips allows one to increase the lateral resolution from micrometers to nanometers. However, feedback-mode constant-height SECM imaging on the nanoscale is challenging because of the possibility of a tip crash. Few examples of such images have been published to date (13). Constant-distance imaging (14) can be used to overcome this problem.

The generation/collection mode imaging with nm-sized probes is easier because the tip/substrate separation distance does not have to be very small. It is useful for mapping fluxes and concentration profiles of electroactive species and studying diffusion and convection processes in electrochemical systems (15) (**Figure 2**).

The highest spatial SECM resolution reported to date was achieved in imaging insulators in humid air (16). In this mode, a conical tip as used for scanning tunneling microscopy partially penetrates an Å-thick aqueous layer that is present on the surface. The tip is scanned over the surface in a constant-current mode to obtain nanoscale topographic images. This arrangement was used to image molecular steps on the mica surface as well as DNA cast on mica. Another approach to nanoscale electrochemical imaging—SECM-AFM imaging (17, 18)—is discussed in Section 8 below.

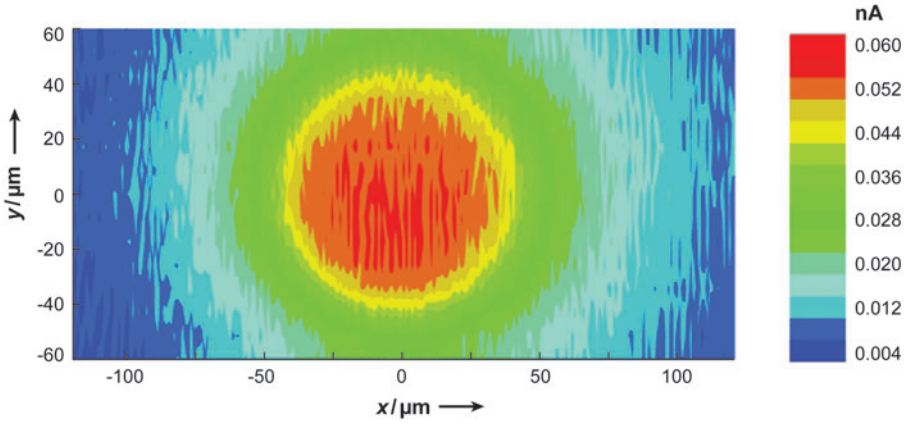

Figure 2

Two-dimensional map of currents (concentrations) measured by an 80-nm tip (collector) in the vicinity of a 40-µm-radius disk electrode (generator). The nanoprobe was scanned parallel to the microelectrode plane at a constant vertical distance $d = 5$ µm with a speed of 8 µm/s. Aqueous solution contained 5 mM $[Ru(NH_3)_6]Cl_3$. The generator potential of the microelectrode was placed on the plateau of the reduction wave of $[Ru(NH_3)_6]^{3+}$, and the nanoelectrode probe potential was set on the plateau of the $[Ru(NH_3)_6]^{2+}$ oxidation wave. Reprinted with permission from Reference 15. Copyright 2004, Wiley-VCH Verlag GmbH & Co. KGaA, Weinheim.

2.5. Feedback-Mode Kinetic Measurements and Single-Molecule Experiments

Feedback mode of the SECM was employed to measure the kinetics of several fast electron transfer (ET) reactions at nm-sized electrodes (8). Polished Pt nanoelectrodes were characterized by a combination of voltammetry, scanning electron microscopy (SEM), and SECM, as discussed above. The substrate was kept at a constant potential, such that the ET reaction at its surface was diffusion-controlled, while the tip potential was swept slowly to record a steady-state voltammogram. A number of voltammograms were obtained at the same nanoelectrode at different tip/substrate separation distances (**Figure 1*c***). In this way, the self-consistent kinetic parameter values for several rapid ET reactions, of which the fastest was $Ru(NH_3)_6^{3+}$–reduction in KCl ($k^\circ = 17.0 \pm 0.9$ cm/s), were obtained at electrodes of different radii (3 to 400 nm) with an uncertainty margin of ~10%.

In single molecule experiments, positive feedback was used to amplify low signals, which were produced by oxidation/reduction of single molecules (19, 20). The active area of a ~15-nm-diameter Apiezon wax-sealed Pt/Ir tip was slightly recessed into the insulating sheath so that, at small tip/substrate distances, solution was trapped in a nm-sized wax pocket between two electrodes. When this tip was held at ~10 nm from the indium-tin oxide (ITO) substrate, the pA-range tip current exhibited slow (on the order of tens of s) fluctuations. Although the signal was noisy, the tip current reproducibly showed peaks of 0.7 and 1.4 pA corresponding to the trapping of one and two electroactive molecules, respectively, and periods of essentially zero average current between them. When the tip potential was swept linearly, the stochastic process produced well-defined steady-state voltammograms with the half-wave potential expected for the employed redox mediator.

3. LIQUID/LIQUID INTERFACE

3.1. Principles

The SECM approaches to probing heterogeneous charge-transfer reactions at the interface between two immiscible electrolyte solutions (ITIES) are similar to those used to investigate solid/liquid electrochemistry (21, 22). To study ET at the ITIES, a UME tip is usually placed in the upper liquid phase (e.g., organic solvent) containing one form of the redox species (e.g., the reduced form, R_1). With the tip held at a sufficiently positive potential, R_1 reacts at its surface to produce the oxidized form of the species, O_1. When the tip approaches the ITIES, the mediator can be regenerated at the interface via the bimolecular redox reaction between O_1 in the organic phase (o) and R_2 in the aqueous phase (w):

$$O_1(\mathrm{o}) + R_2(\mathrm{w}) \rightarrow R_1(\mathrm{o}) + O_2(\mathrm{w}), \qquad (1)$$

and i_T increases with the decrease in the tip/interface distance (positive feedback). The kinetics of such a reaction can be evaluated from approach curves (23).

In the ion-transfer feedback mode, a μm- or nm-sized pipette is filled with a solvent immiscible with the outer solution and used as a tip to approach a macroscopic ITIES.

The interfacial charge-transfer reactions producing the tip current and the feedback are either facilitated (24) or simple (i.e., unassisted) (25) ion transfers rather than ET. Selzer and Mandler (26) used micropipette tips to probe the coupling of ion transfer and ET at the ITIES.

In most SECM experiments, a nonpolarizable ITIES is poised by the concentrations of the potential-determining ion providing a constant driving force for either ET or ion-transfer process. Alternatively, a polarizable ITIES can be externally biased to provide a wider range of interfacial voltages for the study of ET (27) or facilitated ion transfer (28).

3.2. Studies of Electron Transfer

The kinetics of ET between zinc porphyrin dissolved in the organic phase and different aqueous redox species (e.g., $Ru(CN)_6^{4-}$, $Fe(CN)_6^{4-}$, or V^{2+}) were studied at the water/benzene interface (29, 30). The results were in agreement with the main predictions of existing ET theory including the linear dependence of $\log(k_f)$ on the interfacial voltage (Tafel plot) with a transfer coefficient, $\alpha = 0.5$. Similar results were obtained for other ET reactions (21, 31, 32). However, the rate of the reverse reaction between ZnPor and $Ru(CN)_6^{3-}$ was found to be essentially potential-independent at the interfaces between water and three organic solvents of different polarities (33). Barker et al. (34) developed a theoretical treatment of the ET at a nonpolarizable ITIES, in which the finite diffusion rate of the reactant in the bottom phase was taken into account. Using this approach, one can measure much faster ET rate constants at the ITIES (31).

Two predictions of the Marcus theory at the liquid/liquid interface were tested, namely the exponential distance dependence of the ET rate and the inverted region behavior (30). The ET rate decreased with the number of C atoms in the hydrocarbon chain of lipid adsorbed at the ITIES, as predicted by ET theory, and the inverted Marcus behavior was observed. Sun et al. (35) used an externally biased polarizable ITIES to control the ET driving force and also observed the inverted Marcus behavior for different combinations of aqueous and organic redox mediators.

The kinetics of interfacial ET between ferrocene dissolved in ionic liquid and aqueous ferrocyanide was probed and found to follow the Butler-Volmer equation (36, 37). The measured bimolecular rate constant was much larger than that obtained at the water/1,2-dichloroethane interface.

Figure 3 shows two possible experimental setups for studying ET reactions between monolayer-protected gold clusters (MPCs) and redox molecules confined to two immiscible liquid phases by SECM (38, 39). Either MPCs (**Figure 3*a***) (38) or conventional redox molecules (**Figure 3*b***) (39) can be employed as a mediator shuttling the charge between the tip and the ITIES. The latter approach was used to measure the heterogeneous rate constant of the ET between organic soluble Au_{38} clusters and an aqueous $IrCl_6^{2-}$ oxidant.

3.3. Ion Transfer Reactions

In an SECM study of facilitated ion transfer (24), the transfer of K^+ from the nanopipette filled with aqueous solution to the external 1,2-dichloroethane (DCE)

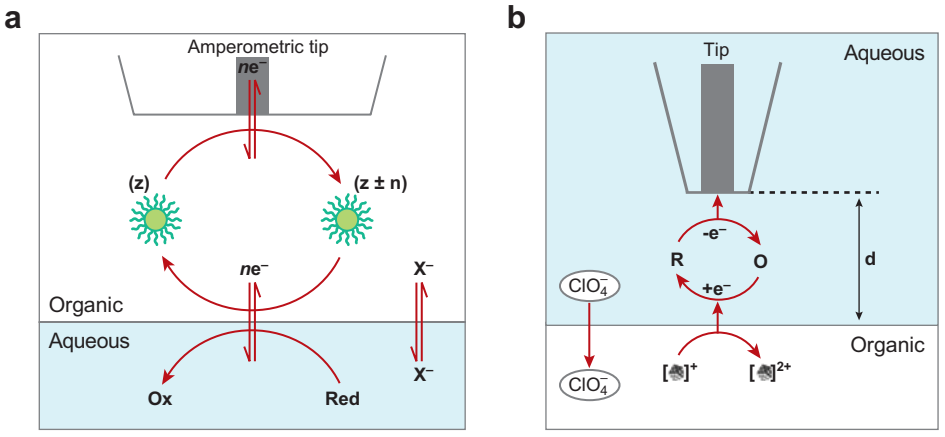

Figure 3

Schematic diagram of two scanning electrochemical microscopy (SECM) approaches to the measurement of the electron transfer rate between an organic-soluble monolayer-protected gold cluster (MPC) and an aqueous redox species. (*a*) The MPC is used as an SECM mediator species. (*b*) Redox molecules shuttle electrons between the tip and the interface between two immiscible electrolyte solutions. Adapted with permission from References 38 and 39. Copyright 2003 and 2004, American Chemical Society.

phase was assisted by dibenzo-18-crown-6 (DB18C6):

$$K^+_{(w)} + DB18C6_{(DCE)} \rightarrow [KDB18C6]^+_{(DCE)} \qquad \text{(at the pipette tip).} \qquad (2)$$

When the tip approached the ITIES, the regeneration of DB18C6 occurred:

$$[KDB18C6]^+_{(DCE)} \rightarrow K^+_{(w)} + DB18C6_{(DCE)} \qquad \text{(at the ITIES),} \qquad (3)$$

and positive feedback current was observed. SECM at an externally biased nonpolarizable ITIES was used to measure the kinetics of Reaction 2 (28). The results were in good agreement with those obtained previously by nanopipette voltammetry at a polarizable interface.

Similar SECM experiments can be performed using a simple IT process (25). In this case, both the top and the bottom phases contain the same ion at equilibrium. The micropipette tip is used to decrease the concentration of this common ion in the top solvent near the ITIES.

Some applications of SECM at the ITIES, e.g., works on molecular partitioning (37, 40), and studies of phase-transfer processes by combination of the SECM with a Langmuir trough (41), could not be covered here because of space limitations.

4. MEMBRANES, THIN FILMS AND SELF-ASSEMBLED MONOLAYERS

4.1. Electron Transfer on Self-Assembled Monolayers

SECM has been used for the studies of electron transfer through monolayers supported at solid/liquid (42, 43), liquid/liquid (44, 45) and air/water interfaces (46). In

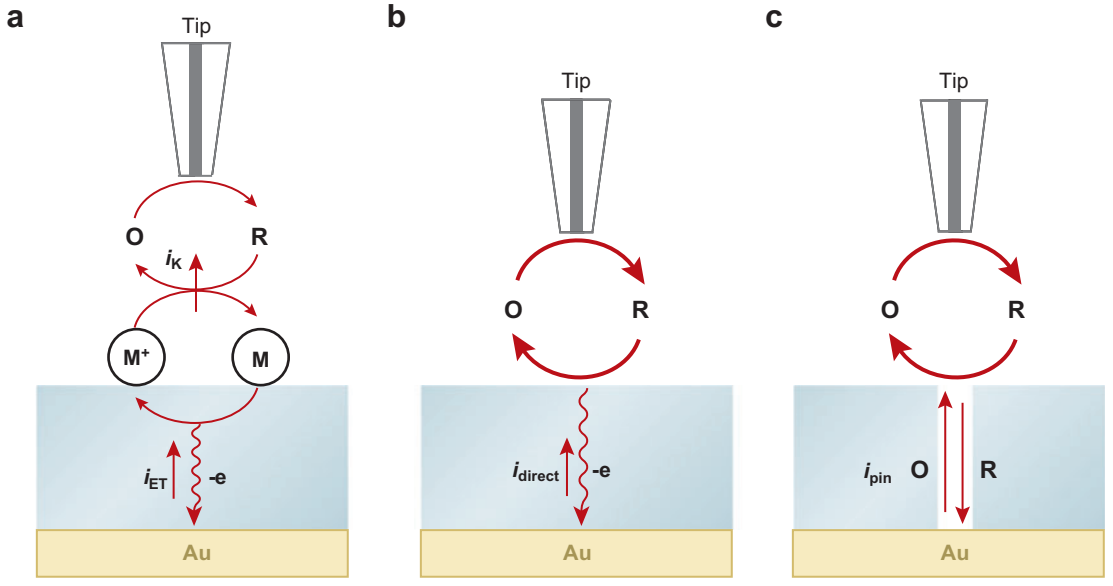

Figure 4

Schematic view of the processes involved in the scanning electrochemical microscopy measurements of electron transfer (ET) across an electroactive self-assembled monolayer: (*a*) mediated ET; (*b*) direct electron tunneling through monolayer; and (*c*) ET through pinholes. Adapted with permission from Reference 42. Copyright 2004, American Chemical Society.

the case of a solid/liquid interface, the rates of ET mediated by monolayer-attached redox moieties and direct ET through the film as well as the rate of a bimolecular ET reaction between the attached and dissolved redox species have been measured using SECM (42). The monolayer may contain redox centers (**Figure 4*a***) or simply act as a blocking layer (**Figure 4*b***).

ET rate kinetics through n-alkanethiol SAMs on Au and Hg have been studied using cyclic voltammetry (47) and SECM and compared with impedance spectroscopy (48, 49) and potentiometry (50). A theoretical model has been developed in an attempt to independently measure the rates of all of these processes (42). According to the model, provided an appropriate mediator is used and the mediator concentration is high such that the bimolecular ET is much faster than the ET through the monolayer, the rate constant of electron tunneling through the monolayer, k_b, is determined by Equation 4:

$$k_b \cong k_{eff} C^* / \Gamma^*, \tag{4}$$

where C^* is the bulk concentration of the redox mediator in solution, Γ^* is the surface coverage of the monolayer-bound redox centers, and k_{eff} is the effective rate constant obtained by fitting an experimental SECM approach curve to SECM theory.

When the tip is very close to the substrate, i.e., $L \ll 1$, L is the normalized tip/substrate distance ($L = d/a$, where d is the distance between the tip and the

substrate and a is the tip radius), the mass transfer coefficient is $m_o \sim D/d$ (where D is the diffusion coefficient), and the upper limit for measurable k_{eff} is $\sim 5m_o = 5\ D/d$. The tip can be brought down to an $L \approx 0.1$. Thus, for a 1-μm-radius tip, $d = 10^{-5}$ cm. Assuming a typical diffusion coefficient $D = 10^{-5}$ cm^2/s, $\Gamma^* \sim 10^{-11}$ mol/cm^2, and $C^* = 2 \times 10^{-4}$ mol/cm^3, the upper limit for measurable k_b is $\sim 10^8$ s^{-1}, calculated using Equation 4. If an nm-sized tip is used, a faster ET can be measured.

On the other hand, if the bimolecular electron transfer is slow in comparison to electron tunneling, and/or the concentration of the redox mediator in solution is low, the following equation holds:

$$k_{Ox} \cong k_{eff}(k_b + k_f)/k_b\Gamma^*, \quad (5)$$

where k_{Ox} is the bimolecular ET rate constant (mol^{-1}cm^{3}s^{-1}), and k_b and k_f are backward and forward electron tunneling rate constants (s^{-1}), respectively. Thus, the bimolecular rate constant for ET between the monolayer-bound and dissolved redox species can be determined based on Equation 5. For a 1-μm-radius tip, the upper limit for measurable k_{Ox} is 10^{11} mol^{-1}cm^{3}s^{-1} (or 10^8 M^{-1}s^{-1}).

4.2. Mass Transfer Across and Lateral Diffusion in Monolayers

SECM (51) allows interfacial dynamics and diffusion to be studied on small length and time scales approaching those relevant to cellular membranes. In recent applications to assemblies at the water/air (W/A) interface, SECM has been used to study lateral proton diffusion along a stearic acid monolayer (46), the effect of a 1-octadecanol monolayer on oxygen transfer across the W/A interface (52), and lateral conductivity in assemblies of metal nanoparticles (53). In these studies, the response of the probe either translated toward or held close to a spot at a target interface was used to obtain quantitative data on a local scale.

For studies involving W/A interface monolayers or Langmuir films, a submarine UME is required. This electrode is immersed in the solution and approaches the layer from below (46, 54). The submarine electrode consists simply of a conventional UME of the desired metal and size fixed to a glass J tube by Teflon tape or epoxy (**Figure 5**); this electrode has also been used for ion channel SECM experiments (55).

Lateral proton diffusion was investigated by steady-state approach curves (51), as surface diffusion contributes primarily to the long-time SECM current response (56). Examples are monolayers comprising either acidic DL-R-phosphatidyl-L-serine, dipalmitoyl (DPPS) or zwitterionic L-R-phosphatidylcholine, dipalmitoyl (DPPC) at a range of surface pressures (57). Typical results, as shown in **Figure 6*a***, indicated an enhanced reduction current for the probe approaching the DPPS monolayer. These results were attributed to lateral proton diffusion providing an additional proton source, which is detected by SECM proton feedback mediated through $H_2PO_4^-/HPO_4^{2-}$. In contrast, approach curves for both a native W/A interface (**Figure 6*a***) and a DPPC monolayer (**Figure 6*b***) showed a current response due only to the diffusion of $H_2PO_4^-$ through solution. For comparison, **Figure 6** also shows the simulated behavior for the DPPS system when the lateral proton diffusion coefficient is comparable

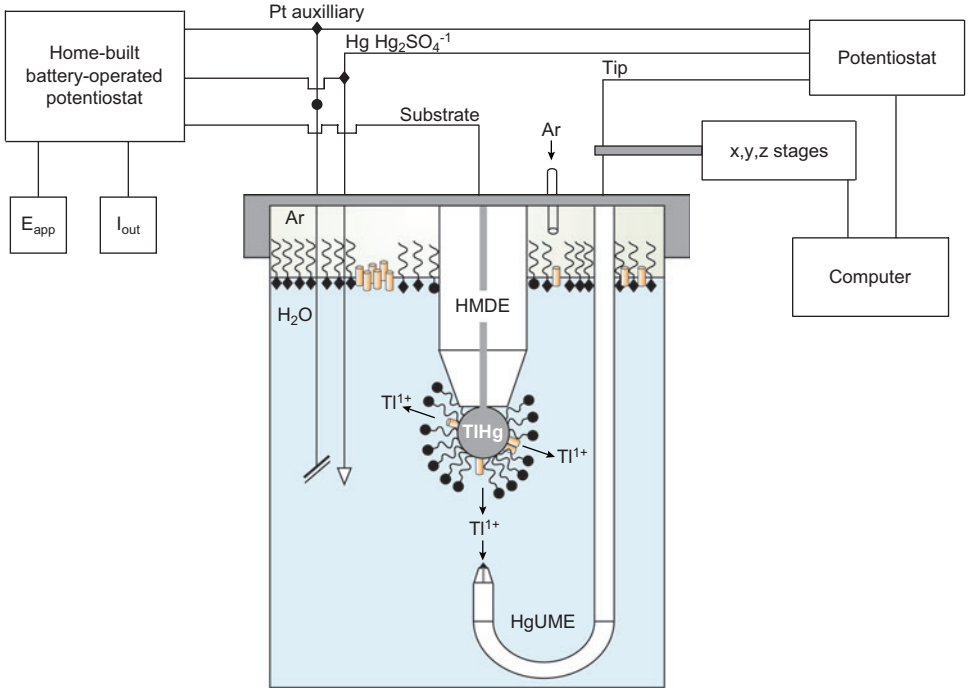

Figure 5

Schematic diagram of an ion channel scanning electrochemical microscopy experiment where a submarine ultramicroelectrode is used. Adapted with permission from Reference 55. Copyright 2002, American Chemical Society.

to the bulk proton diffusion coefficient. In this case, a significant increase in current is predicted as the probe approaches the monolayer that was not observed experimentally. Lateral proton diffusion coefficients at DPPS derived from approach curve measurements are summarized in **Figure 6*c***. As the surface pressure increased from 1 to 20 mN/m, the lateral proton diffusion coefficient, D_{lat}, increased from approximately 1.5×10^{-6} cm^2 s^{-1} to 6×10^{-6} cm^2 s^{-1}. At the higher pressures, where A changed only slightly, the lateral diffusion coefficient was reasonably uniform.

4.3. Mass Transport through Phospholipid Monolayer, Bilayer Lipid Membrane, or Liposome

The self-assembling ability of amphiphilic molecules, such as phospholipids, to form bilayers has been widely studied because of the similar physical properties of such artificial membranes and membranes found in biological cells (58). Tsionsky et al. (59) first used SECM to study the kinetics of charge-transfer processes at bilayer lipid membranes (BLMs). Analysis of the SECM tip response demonstrates that an unmodified BLM behaves as an insulator, whereas a BLM doped with iodine shows some positive feedback. Later, using a similar setup, a voltammetric K^+-selective

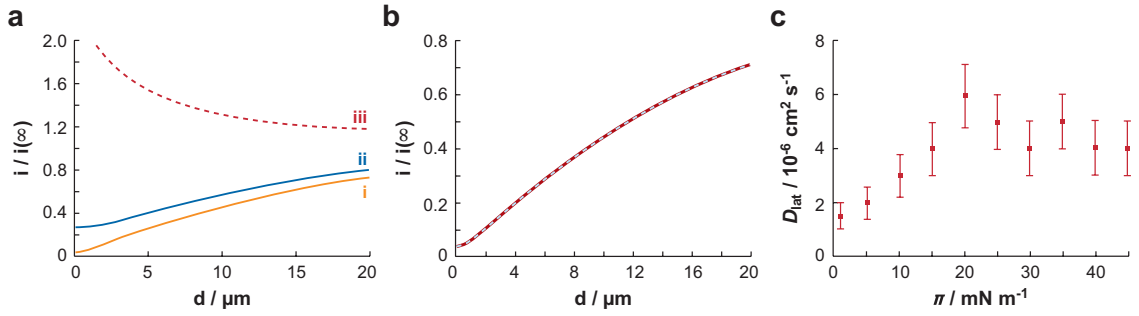

Figure 6

Typical approach curves for the measurement of lateral proton diffusion. (*a*) The solid experimental curves are for the reduction of 0.5 mM $H_2PO_4^-$ at a UME approaching (*i*) a native W/A interface and (*ii*) a DPPS monolayer (p = 20 mN m^{-1}). The dashed curves represent simulations for (*i*) an inert interface; (*ii*) the DPPS system with $D_{lat} = 6 \times 10^{-6}$ cm^2 s^{-1} ($A = 50$ Å^2); and (*iii*) $D_{lat} = 1 \times 10^{-4}$ cm^2 s^{-1} ($A = 50$ Å^2). (*b*) The experimental curve for a DPPC monolayer (*solid*) was similar for all pressures ($p = 1$, 5, 10, 20, 30, and 40 mN m^{-1}) and the dashed curve (coincident) represents the simulation for an inert interface. (*c*) D_{lat} as a function of surface pressure, p, derived from approach curve measurements for the DL-R-phosphatidyl-L-serine, dipalmitoyl system. Adapted with permission from Reference 57. Copyright 2002, American Chemical Society.

micropipette electrode based on valinomycin and ETH 500 in dichloroethane was used as the probe to study K^+ transfer through gramicidin channels in a horizontal BLM in the SECM feedback and generation-collection modes (60).

The difficulty with this measurement is controlling the time at which the ion transport occurs. To have a controlled release of the ion of interest, an amperometric approach can also be used but requires the use of Tl(I) as a surrogate for K^+. Ion transport across gramicidin channels embedded in a dioleoylphosphatidylcholine monolayer adsorbed onto a Tl/Hg amalgam can be used as a membrane system. This arrangement allows one to control the release of Tl(I) into gramicidin channels by preconcentration of the Tl as an amalgam on a hanging mercury drop electrode with controlled oxidation of the amalgam using a potential step. An Hg/Pt submarine UME positioned close to the membrane, as shown in **Figure 5**, collects the generated Tl(I) following its diffusion from the gramicidin.

Giant liposomes encapsulating redox molecules have also been prepared and probed by SECM using sub-μm conical carbon fiber tips, which were employed to approach, image, and puncture individual liposomes (5). Characteristic breakthrough (puncture) current transients corresponded to liposomes of different compartmental configurations, and voltammetric curves with the tip inside the liposome were obtained. The leakage of the encapsulated redox molecules from liposomes was also studied by positioning electrodes close to (<200 nm) the surface of a single liposome.

As shown in **Figure 7** (*right*), different characteristic breakthrough curves were observed, consistent with the different cases shown schematically in **Figure 7** (*left*) (5). In all three cases shown in **Figure 7**, a decrease of current was first observed as the tip traveled down to the surface. After the apex of the tip touched the membrane,

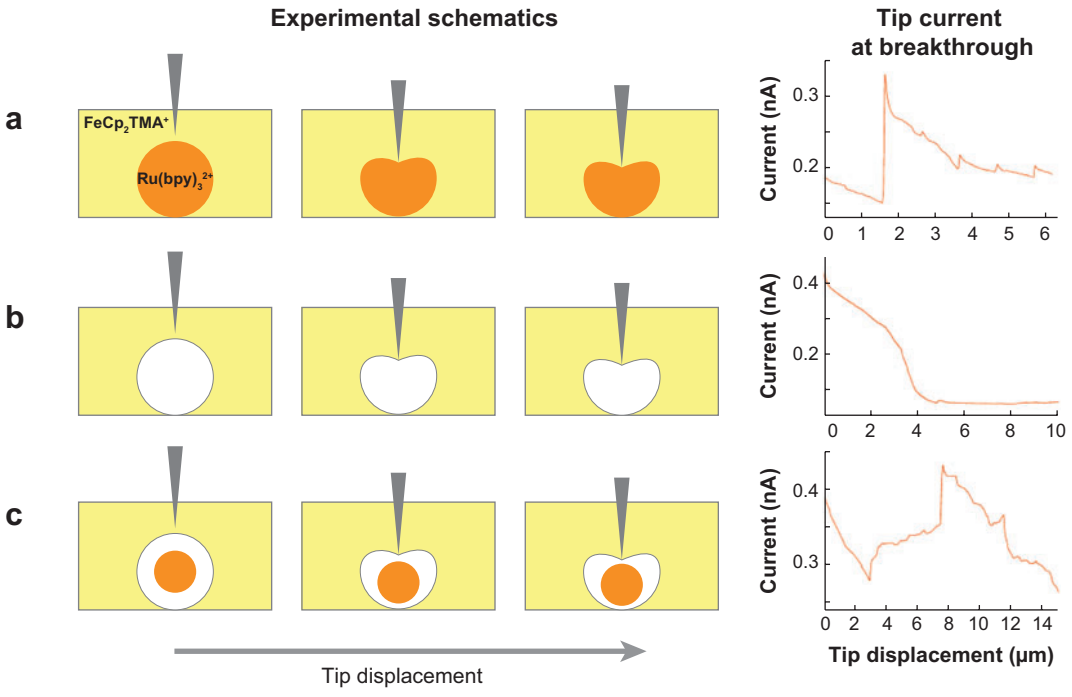

Figure 7

(*Left*) Schematic presentation of different liposomes that undergo shape deformation during the course of tip breakthrough experiments (from left to right). Liposomes are divided into three kinds based on their $Ru(bpy)_3^{2+}$ content and distribution. (*Right*) Scanning electrochemical microscopy monitoring of tip current when it breaks through the bilayer(s) of different liposomes, corresponding to each of the schematics. In this series of experiments, the tip potential was held at 1.2 V (versus AgQRE) where $Ru(bpy)_3^{2+}$ is oxidized to $Ru(bpy)_3^{3+}$. The regular, 1-μm-spaced current spikes in the approach curves are due to the mechanical clicks of the inchworm motor used. A 1-mM ferrocenylmethyltrimethylammonium perchlorate ($FeCp_2TMA^+$) in Tris-HCl buffer (10 mM Tris and 0.1 M NaCl, pH 7.0) was used as the redox mediator. Adapted with permission from Reference 5. Copyright 2006, American Chemical Society.

a further lowering of the tip deformed the lipid bilayers downward, accompanied by a further drop of the current. This effect is reminiscent of the SECM behavior noted when a tip approaches the interface between an aqueous solution and an immiscible liquid and a thin layer of solution is trapped. The breakthrough of the liposome normally took place a few micrometers below the point where the tip first touched the liposome surface, which varied from one experiment to another due to differences in the tip sharpness and liposome size.

At the breakthrough point, a transient with a sharply rising current was obtained for a liposome [**Figure 7** (***right***, **panel *a***)]. This event was attributed to the sudden immersion of the tip into a solution of $Ru(bpy)_3^{2+}$ and a Cottrell current transient along with a contribution from charging current. For a liposome that did not contain

electroactive species, $Ru(bpy)_3^{2+}$, a decrease of current was observed on breakthrough [**Figure 7** (***right***, **panel *b***)] (5). A rise of current was only observed following a decrease in current [(**Figure 7** (***right***, **panel *c***)] when the tip broke into the core of a multilamellar liposome whose core was filled with $Ru(bpy)_3^{2+}$.

4.4. Transport Activity in Thin Films or Membranes

In one type of SECM study on thin films or membranes, the tip is held at a potential where it can detect an electroactive ion released from the film during a redox process (61–63). For example, SECM was used to detect the release of Br^- during the reduction of oxidized polypyrrole (PP), in the form of PP^+Br^- (63). During a reductive cyclic voltammetric scan, Br^- was found to be released after an appreciable amount of cathodic charge had passed, suggesting that during the early stage of the reduction the uptake of cations, rather than the release of anions, maintained charge balance in the film.

The SECM studies of polymer films described above rely on using the tip to probe the solution environment directly above the polymer to investigate electron transfer and ion ejection and incorporation into the film. SECM can also be used for direct electrochemical measurements by recording the tip current and CVs as the tip is moved from the solution into the polymer phase and ultimately contacts the substrate. (See Section 2.3 for more detailed discussion.)

Early SECM work on the studies of charge and mass transport activity of membranes has been extensively reviewed by Bath et al. (64). We mainly focus here on work carried out since then. Recently, SECM utilizing an amperometric microbiosensor based on coimmobilization of the enzymes glucose oxidase and hexokinase has been applied for imaging ATP transport through a porous polycarbonate membrane under physiologically relevant conditions (65). Integration of the amperometric ATP microbiosensor into a dual-microdisk electrode configuration has been achieved by immobilizing the enzymes at one of the microdisk electrodes while the second disk serves as an unmodified amperometric probe for controlled positioning of the microbiosensor in close proximity to the sample surface, enabling quantification of the obtained current signal. SECM operated in feedback mode has also been used in combination with silver nanoparticles–tagging to achieve visualization of proteins adsorbed on a polyvinylidene difluoride (PVDF) membrane, which was detected with osmium tris-bipyridine as a redox mediator in aqueous solution (66).

Another application of SECM is to investigate counter-ion transport through four different proton-conducting membranes with poly(styrene sulfonic acid) side chains (67). These membranes, intended for the polymer electrolyte fuel cell, are based on PVDF and PVDF-co-HFP matrix materials and have been prepared by an irradiation grafting method. SECM is found to be suitable for mapping variations in proton diffusion coefficient and concentration in these inhomogeneous membranes.

In their investigations of membrane transport, White et al. (68, 69) developed two imaging modes. In the forward imaging mode (FIM), the SECM tip is placed in the receptor compartment and poised at a potential such that the electroactive molecule is oxidized or reduced as it emerges from pores in the membrane. In the reverse imaging

mode (RIM), the diffusion of molecules into the pore depletes solute in the donor solution immediately adjacent to the pore entrance, resulting in a decrease in the tip current as the tip is rastered across the area above the pore. In principle, RIM has an inherently lower sensitivity than FIM because the signal is measured relative to a large background. However, RIM provides a means of imaging molecular transport into biological membranes, which is not possible using FIM (68). This is a key advantage for monitoring the uptake of molecular species into single cells and biological tissues.

SECM imaging of a membrane containing conical-shaped pores (60-nm and 2.5-μm diameter openings) by alternating current (ac) impedance mode has been demonstrated (70). Impedance images of the pore openings were obtained by rastering a glass-sealed conical-shaped Pt tip (~1-μm radius) above the membrane surface, while measuring the total impedance between the tip and a large-area Pt electrode located on the opposite side of the membrane. Image contrast in ac impedance SECM of membranes increases dramatically as the membrane resistance decreases. Experiments and theory (71) demonstrate that, in instances where the SECM tip resistance is small relative to the internal pore resistance, the total impedance changes by a negligible amount during imaging, resulting in insufficient image contrast to obtain images. As reported (71), a simple and highly effective solution to this problem is to shunt the ion current around the membrane using a low-impedance bypass channel.

Finally, conductance measurements at solid/liquid interfaces with scanning probes are interesting, especially under conditions in which the ionic species under investigation are not electroactive. Besides those ac impedance techniques described above (72–74), a bipolar conductance (BICON) technique for the measurement of solution resistance by SECM was used (75), based on the application of μs-current pulses originally described by Enke et al. (76) for measurements with conventional electrodes. This technique was applied to measuring conductance changes during irradiation of photoresist film in 18-MΩ-cm water, an important process in immersion lithography (77). BICON/SECM approach curves over insulating substrates followed SECM negative feedback theory. Approach curves to a conducting substrate at open circuit potential are influenced by the solution time constant (i.e., solution resistance at the tip multiplied by electric double-layer capacitance), which is a function of tip/substrate distance as well as the substrate size (75). With BICON/SECM, it is possible to obtain approach curves in solution with no intentionally added electrolyte; however, its sensitivity limit is only in the micromolar region (77).

5. BIOLOGICAL CELLS

In recent years, SECM has been extensively applied to studies of a variety of biological cells (78–81). In these new biological applications of SECM, a chemical substance that participates in a cellular process is monitored selectively and sensitively to obtain quantitative information of biological significance. A single cell, under either a closely packed or an isolated condition, can be identified utilizing SECM imaging with μm/subμm spatial resolution. Moreover, without any cellular fixation or invasion, chemical reactivity of a living cell can be investigated in real time by SECM.

These unique advantages, illustrated by the following examples, make SECM a powerful tool for biological and biomedical research.

5.1. Single-Cell Viability

The viability of single cells can be assessed by SECM on the basis of their respiration activity. Employing *x-y* SECM scans, a tip current based on oxygen reduction decreased near living human colon cells because of oxygen consumption in cellular respiration (82). Spatial resolution and sensitivity of SECM were high enough to image an oxygen concentration profile for individual cells. Recently, the noninvasive SECM measurement of respiration activity was applied to the monitoring of oxygen consumption by identical bovine embryos during their development under a cultured condition (83). The oxygen consumption rate at the initial developing stage was found to be a measure of embryo quality.

Effects of toxic substances on the viability of a HeLa cell were monitored by SECM (84). The cell was loaded with a Calcein dye for a simultaneous fluorescence viability assay. Upon exposure to CN^-, which functions as a respiration inhibitor, the oxygen concentration around the cell increased immediately and reached a bulk concentration after 30 min. After the complete loss of respiration activity, the fluorescence intensities at each cell declined, thereby indicating that the dye had leaked through collapsed cell membranes. On the other hand, an SECM measurement was necessary to detect cytotoxicity of antibiotic Antimycin A, addition of which to a HeLa cell resulted in immediate respiration breakdown without membrane deformation for at least 2 h.

SECM was also applied to the investigation of interactions of fibroblast cells with micromolar amounts of Ag^+ known as antibiotics (85). An Ag^+ concentration profile around a single cell was monitored using an amperometric ion-selective probe based on a calixarene-type Ag^+ ionophore. A comparison between SECM images and SEM images revealed that Ag^+ had accumulated in the cell nucleus.

5.2. Cellular Redox Activity

SECM was utilized to distinguish between metastatic and nontransformed human breast cells by their redox activity (86). In the SECM feedback measurements, a hydrophobic redox mediator was electrolyzed at the electrode tip so that a tip-generated species entered a cell and was oxidized or reduced at intracellular redox centers. Using menadione as a mediator, a smaller feedback effect was observed when comparing a metastatic cell with a nontransformed cell. A detailed mechanistic study demonstrated that the smaller redox response for a metastatic cell was due to a lower intracellular concentration of oxidative moieties available for menadione regeneration (87). The suppressed redox activity was related to high endogenous levels of protein kinase Cα in a metastatic cell; this lower activity was also observed with a human breast cell engineered to overproduce the protein kinase. In fact, expression of cellular reductants such as NAD(P)H:quinone oxidoreductase was induced by the protein kinase, thereby resulting in the diminished oxidative activity (88).

SECM imaging of a mixed field of metastatic and nontransformed cells allows for identification of metastatic cells on the basis of their lower reactivity to

quinone mediators (89). Such a redox activity map was obtained using SECM imaging and confirmed using a fluorescence microscopic assay, where cancer cells were tagged with fluorescent nanospheres without alteration of their redox activity. Interestingly, a cellular redox response to a mediator, *N*,*N*,*N*′,*N*′-tetramethyl-1,4-*p*-phenylenediamine, was found to depend on the cell density. Whereas densely packed cancer cells became slightly more active, the redox activity of nontransformed cells decreased in a confluent culture, suggesting contact inhibition of cellular metabolism (88).

5.3. Channel-Mediated Membrane Transport

Membrane transport mediated by protein channels/pumps is crucial for cellular functions. SECM was applied to the investigation of menadione metabolism by monitoring the export of a menadione-glutathione conjugate, i.e., thiodione, by an ATP-dependent pump. Exposure of yeast cells to menadione was immediately followed by the active export of thiodione (90). A thiodione efflux was measured amperometrically and analyzed using a constant flux model, yielding an average single cell flux of 3×10^4 molecules/s. The active thiodione export was also investigated for hepatoblastoma (91). Successive SECM images of a single Hep G2 cell were obtained (**Figure 8**) to demonstrate that a thiodione efflux decreased gradually to fall below detectable limits after 1 h. This result agrees well with a cytotoxicity assay.

Passive molecular transport through the nuclear pore complex (NPC) was investigated by SECM (92). The NPC is a large protein complex that exclusively mediates molecular transport across the nuclear envelope between the nucleus and the cytoplasm. SECM approach curves at intact nuclei isolated from *Xenopus laevis* oocytes

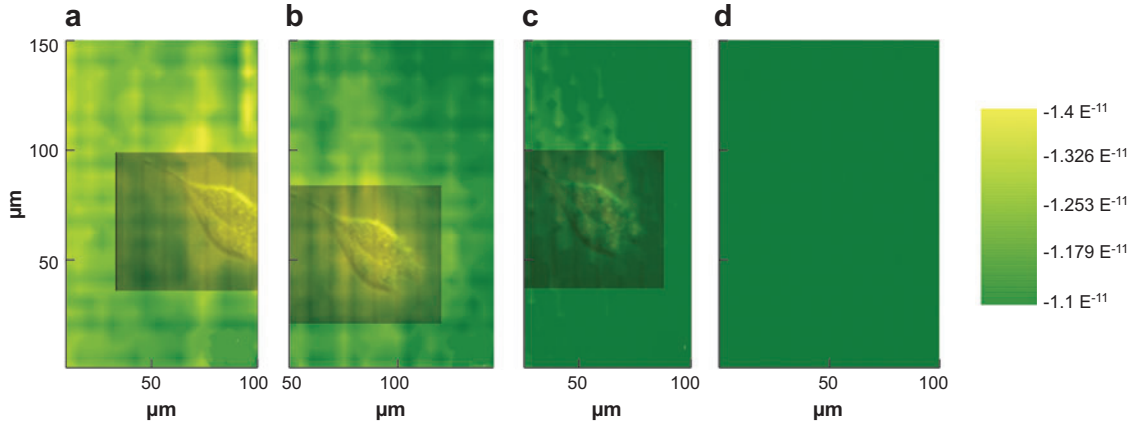

Figure 8

Superimposed optical micrographs on the corresponding scanning electrochemical microscopy (SECM) images based on thiodione export from the Hep G2 cells (91). The SECM images were obtained successively (panels *a–d*). It took ~7 min to acquire each image. Adapted from Reference 91 with permission. Copyright 2004, National Academy of Sciences, USA.

demonstrated that the permeability of the nuclear envelope to small redox molecules such as ferrocene derivatives is at least two orders of magnitude larger than the permeability of BLMs and cell membranes to the same molecules. The large permeability, which was noninvasively determined by SECM, is consistent with the high density and large size of open NPC pores.

5.4. Imaging Model Neurons

Sophisticated imaging techniques were developed to map the exocytosis of neurotransmitters from individual vesicles at cultured model neurons (93). High-resolution imaging of model neurons with high relief requires dynamic tip positioning at a short and constant distance from the cell surface. A shear force between the tip and the cell was utilized as a feedback signal for constant-distance control (93). A topographic image of a PC12 cell was obtained by employing the constant-force mode, where a resonant frequency of a vibrating carbon fiber probe was monitored to maintain a constant shear force. Neurotransmitters released from individual vesicles were detected amperometrically by positioning the tip above the cell surface in the constant-force mode. A fluorescence viability assay confirmed that PC12 cells were not damaged during shear force–based topographic imaging (94).

An electrochemical tip response can also be used for distance control (95). In constant-current mode, the tip is moved vertically during an *x*-*y* scan so that a constant tip current generated from the electrolysis of redox molecules is maintained. A detailed topographic image of a differentiated PC12 cell was acquired using the constant-current mode (**Figure 9**), clearly demonstrating the height differences at the cell body and neutrites. Alternatively, a constant distance can be maintained by monitoring the tip impedance as a feedback signal. In contrast to the constant-current

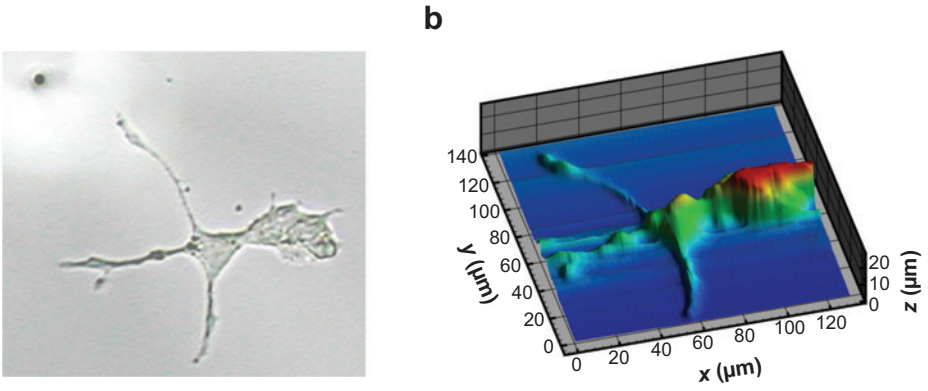

Figure 9

(*a*) Optical and (*b*) constant-current topographic images of a differentiated PC12 cell (95). The scanning electrochemical microscopy image was acquired using a ~1-µm-diameter carbon ring electrode and 1.0-mM $Ru(NH_3)_6^{3+}$ mediator. Adapted from Reference 95 with permission. Copyright 2005, American Chemical Society.

mode, the constant-impedance mode allows for simultaneous amperometric recording of neurotransmitter releases.

5.5. Advanced Electrochemical and Optical Imaging

The combination of SECM and optical microscopy is a powerful approach to obtaining multidimensional information about complicated cellular processes. An SECM stage mounted on an inverted optical microscope is a standard setup for simultaneous electrochemical and optical imaging. Recently, such a setup permitted a single-molecule fluorescence study of F_0F_1-ATP syntheses in liposomes (96). ATP synthesis was driven by a local pH gradient created by H^+ reduction at an SECM tip. The resulting intersubunit rotation within a single enzyme molecule was able to be monitored by intramolecular fluorescence resonance energy transfer with a confocal laser microscope.

A ring UME based on an optical fiber was developed as a probe of a combined scanning electrochemical/optical microscope (97). An optical image of freshwater diatoms, *Navicula minima*, was obtained using the optical fiber probe as a light source. At the same time, a topographic image of the soft biological samples was obtained in the constant-current mode, yielding better image quality than in the constant-force mode. Moreover, a recent study demonstrated single-cell imaging by SECM integrated into a commercial near-field optical microscope, which also has the capabilities of atomic force microscopy (AFM) and confocal microscopic measurements (98). Construction of a smaller optical fiber probe will enable nm-resolution electrochemical and optical imaging.

6. ELECTROCATALYSTS AND SCREENING

6.1. Basic Concepts of High-Throughput Screening of Electrocatalysts

The search for new materials for electrochemical applications (e.g., electrocatalysts for complex electrode reactions like the oxygen reduction reaction (ORR), hydrogen or methanol oxidation reactions for fuel cells, or the water oxidation reaction for photoelectrochemical systems) continues to be an important activity. SECM has found growing application in this area, as it is excellent for rapid screening of arrays of materials and directly produces electrochemical data that can be used as quantitative estimates of rate and activity. This approach is somewhat different than the traditional one where one carefully synthesizes and characterizes a material and then tests it on a macroscale, for example with the rotating disk electrode, but it allows one to screen a large number of different compositions rapidly. Of equal importance to the screening is the rapid preparation of the arrays to yield small samples (spots or lines) that are of reasonably uniform, but varying, composition on a substrate that has very low electrocatalytic properties. This section reviews briefly the principles involved in such studies and examples of the work that has been carried out in this area.

6.2. Fabrication of Arrays

To be a useful technique for high-throughput screening, arrays of samples should ideally be capable of being prepared in an automated way, rapidly and inexpensively, while covering a wide range of compositions, with good reproducibility of the test spot composition. Numerous different array substrates and methods of preparation for use in SECM have been reported. These are summarized in **Table 1**.

A substrate that uses individually addressable spots would, in principle, allow the closest control of each location potential and thus the smallest background current, as the substrate itself and all of the spots except the one addressed by the tip would not contribute to the substrate current. For example, an array of 25 Pt spots, 10 μm in diameter and spaced 100 μm apart, has been imaged by SECM using ferrocene methanol as a mediator with all of the spots at the same potential or at open circuit (99). However in a rapid screening mode, one would have to synchronize the application of potential at the spots with the tip position over a given spot by some sort of potentiostat multiplexing arrangement. Moreover such arrays are relatively expensive. To date, such arrays have not been used for SECM screening purposes. This is similarly true for an array of eight individually addressable lines, 25 mm long, 1 mm wide, and with a 1.5-mm separation formed on an indium-tin oxide electrode by photolithography and etching (100). In this case the individual elements could be plated with different compositions Pt_xRu_y by controlling the potential of one element at a time and changing the solution for electrodeposition. However, in SECM screening all of the elements were maintained at the same potential.

The usual approach is to use a single substrate material, often carbon or ITO, that shows poor catalytic properties (so the background current density at an interspot region is small) and prepare an array of spots or lines thereon. This approach was used to prepare bi- and trimetallic spots on glassy carbon (GC) substrates (105–107). This made use of a piezo dispenser that could deliver pL-drops of appropriate

Table 1 Representative approaches to forming sample arrays[a]

Substrate	Composition and deposition method	Reaction studied	Reference(s)
Addressable array, Pt	Pt, proof of concept (5 × 5 array)	FcMeOH, feedback, SG/TC	99
Patterned ITO	$Pt_xRu_yMo_z$, electrodeposition (8 lines)	H_2 oxidation, feedback	100
Au	Pt, electrodeposition proof of concept	H_2 oxidation, feedback	101
ITO	Pt_xRu_y, gradient, agar, electrodeposition	H_2 oxidation, feedback	102
ITO	Pt coverage, gradient, electrodeposition	H_2 oxidation, feedback	103
HOPG	Pt, random, drop coating	H^+ reduction, feedback, TG/SC	104
GC	Pd_xM_y (M=Co, Ti), PZT dispenser	O_2 reduction, TG/SC	105–107
GC	Cu(II)-polyhis films, PZT dispenser	O_2 reduction, TG/SC	108
GC	Hydrogels, wired enzymes (laccase)	O_2 reduction, TG/SC	109
Si, TiN layer	Pt_xRu_y, sputtering	H_2 oxidation, feedback	110

[a]Abbreviations: ITO, indium-tin oxide; HOPG, highly ordered pyrolytic graphite; GC, glassy carbon; PZT, piezoelectric; TG/SC, tip generation/substrate collection; SG/TC, substrate generation/tip collection.

solutions of the metal salts that were computer-controlled to move and dispense at precise locations. After one metal salt was deposited, the solution was drained from the dispenser and a second metal salt solution (and perhaps a third) was used over the same array. This resulted in an array of drops containing different programmed amounts of the metals. These were vortex mixed and then treated with H_2 at an elevated temperature to produce alloy spots. Alternatively, one can use sodium borohydride solution for the reduction. The exact solution composition (choice of metal salt and solvent) and the array-processing procedure are important for obtaining reproducible and well-formed electrocatalyst spots (106).

A similar approach utilizing a single inert substrate (GC) and piezo dispensing was used with enzymes and biomimetic-type spots (108, 109). Instead of the piezo dispenser, one can also employ an ink jet printing device such as those used in combinatorial array preparations with other methods of screening. A disadvantage of approaches using a common conductive substrate is that the background current from this material can be significant. However, one can prepare a covering layer of an insulator such as Teflon with holes for the spots, which is much simpler than preparing an individually addressable array (J. Rodriguez and A.J. Bard, unpublished experiments).

An alternative approach to preparing different electrocatalysts is to prepare a continuous gradient of compositions. This has been accomplished with electrodeposition across a resistive element (101, 102), by changing the composition of a thin-layer film (e.g., agar) by controlled solution treatment, or by sputtering (110).

6.3. Screening by Scanning Electrochemical Microscopy

As illustrated in **Figure 10**, there are four different SECM approaches to examining electrocatalysis on a substrate. Determining which technique to employ depends upon the reaction to be studied at the substrate and whether the reactant of interest can be generated at the tip. Each approach is briefly discussed and some examples of their use are given.

6.3.1. Feedback approach. If the species to be studied at the substrate can be generated at the tip so that the redox pair of interest represents a typical SECM mediator, the effect of substrate potential, E_S, on the tip current, i_T, can be used to determine the activity of the substrate and the heterogeneous rate constant. Consider the examination of electrocatalysts for H_2 oxidation (110–112): The tip is held at a potential where H^+ is reduced at the diffusion controlled rate in a solution where its concentration is ~0.01 M. This concentration is consistent with typical SECM measurements and is at a value where the H_2 generated does not form bubbles, but rather dissolves in the solution and diffuses to the substrate. As with other kinetic studies by SECM, approach curves as a function of substrate potential allow one to calculate the heterogeneous rate constant, $k(E)$. Similarly, a substrate can be scanned at a constant d to determine relative activities. A disadvantage of this approach is that one is limited to a rather small range of H^+ concentration (or pH). At much lower concentrations the currents become too small to measure above background, and at higher concentrations hydrogen

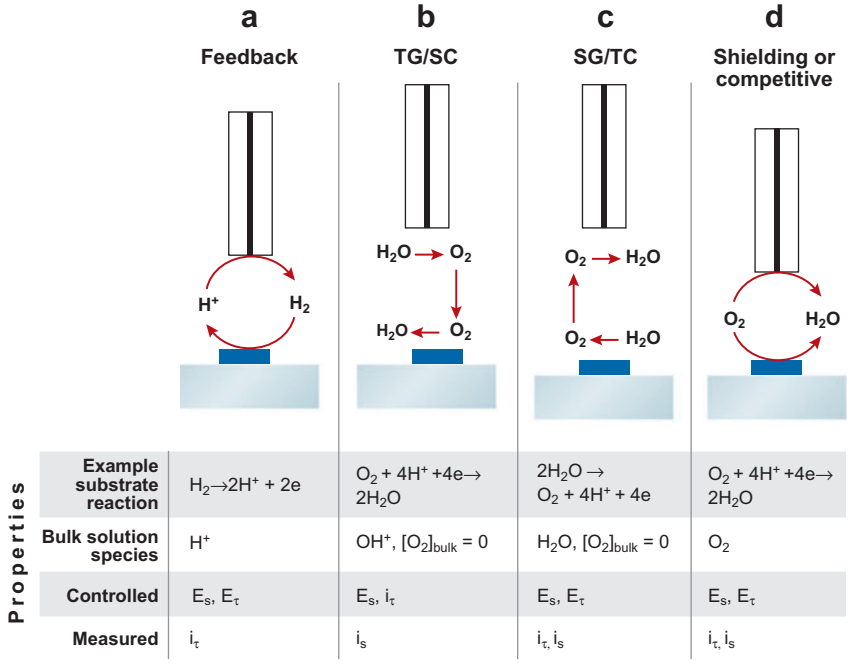

Figure 10

Schematic representation of different modes of substrate screening in scanning electrochemical microscopy. TG, tip generation; SC, substrate collection.

bubbles form. The effect of other species on the reaction, such as CO, can also be studied (112). A similar approach can be used to study the O_2 reduction reaction at the substrate by oxidation of 0.01 M OH^-, which is oxidized before water oxidation, at the tip (113). Again, one is limited to a rather small pH range and therefore would be unable to study the ORR in 0.1 M acid, which would be a more appropriate medium for fuel cell studies.

6.3.2. Tip generation/substrate collection. An alternative approach wherein the tip generates the substrate reactant with considerably more flexibility is tip generation/substrate collection (TG/SC) (**Figure 10*b***) (106, 114, 115). In this approach i_T is controlled, usually as a constant current that generates a constant flux of reactant. When the tip is close to the substrate and the array spots are sufficiently far apart, only the spot immediately below the tip is addressed. The substrate current at that spot at a given potential is a measure of the activity of the spot. For example, for a study of the ORR at the substrate, the solution is de-aerated so that the bulk concentration of O_2 is low. Then O_2 is generated at the tip and reduced at the substrate and the *x*-*y* scan shows i_S as a function of position and potential (105–107, 116). A typical result for Pd-Co electrocatalysts for the ORR is shown in **Figure 11**.

6.3.3. Substrate generation/tip collection. The above approaches are not available under some circumstances, for instance screening an array with electrocatalysts for water oxidation (**Figure 10*c***). One cannot generate the reactant, water, in an aqueous

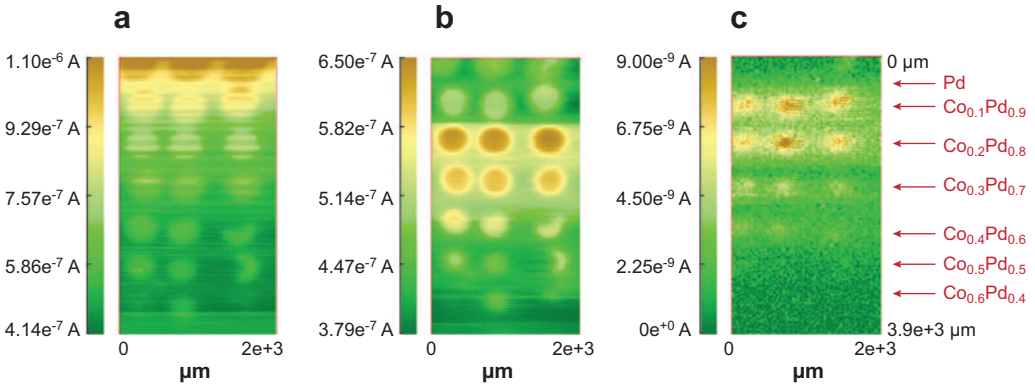

Figure 11

Scanning electrochemical microscopy tip generation/substrate collection images for the oxygen reduction reaction for an array of Pd_xCo_y spots on glassy carbon in 0.5 M H_2SO_4. Oxygen generated at the tip (25-µm diameter W) at a constant current of 183 nA and reduced at the spots with substrate potentials of (*a*) 0.2; (*b*) 0.45; and (*c*) 0.7 V versus standard hydrogen electrode (SHE). Distance between tip and substrate, *d*, is 50 µm. Tip scanned in *x*-*y* plane at 600 µm/s. Adapted from Reference 106 with permission. Copyright 2007, American Chemical Society.

solution at the tip nor involve it in a feedback arrangement. In this case, substrate generation/tip collection (SG/TC) can be used, where the substrate potential is held at different potentials and O_2 is detected at the tip (A. Minguzzi, S. Rondinini, and A.J. Bard, unpublished experiments). In this approach, one cannot have O_2 in the bulk solution and must provide for its removal or another method of preventing interference from O_2 generated at neighboring spots.

6.3.4. Shielding (competitive). If the species to be tested cannot be conveniently generated at an electrode and no product of the electrode reaction can be detected, e.g., with methanol, it is still possible to test an array using SECM shielding. In shielding, the same reaction occurs at the tip and the substrate, so that the current at the tip is decreased compared to what would be observed with an insulating substrate (117, 118), i.e., the tip is shielded by and competes with the substrate for the same reactant (**Figure 10*d***). Thus, a reactant in bulk solution can be studied by noting how well the substrate competes with the tip for consumption (e.g., oxidation of methanol) of the reactant. This approach was used to study the ORR as an alternative to TG/SC (119, 120).

7. PROPERTIES AND REACTIVITY OF MATERIALS

The ability of SECM to map physicochemical processes at interfaces has proved particularly powerful in elucidating the local properties and reactivity of a wide variety of materials. Applications in this area continue to expand and embrace metals,

semiconductors, electrically insulating inorganic and organic materials, soft matter, immobilized nanoparticles, and nanotubes.

7.1. Redox Activity of Complex Electrode Surfaces

The application of SECM to the investigation of the heterogeneous activity of electrodes is well illustrated by studies of conducting (boron-doped) polycrystalline diamond (BDD) (121–123). This material is attracting attention as a novel electrode due to its wide potential window in many solvents and resistance to fouling in complex media, among other attributes. BDD has often been treated as uniformly active, but SECM studies of several sources of synthetic diamond (with varying dopant levels and surface termination) have demonstrated that different grains in polycrystalline BDD show characteristics that depend on the dopant level of individual grains (121–123). SECM data (approach curves, feedback imaging, and SG/TC measurements) have been linked to results from complementary techniques, such as conducting probe (CP)-AFM, cathodoluminescence imaging, and Raman microscopy on the same areas of samples to provide a wealth of quantitative information on the nature of active sites. These studies have demonstrated how the local composition of a grain and its properties influence the electrochemical response (122, 123).

SECM has proved especially powerful in identifying precursor sites for corrosion in otherwise passive oxide films that protect certain metals and alloys (124–126). In these studies, the substrate of interest is generally biased to carry out a redox reaction and the imaging SECM tip detects the product of the reaction, thereby allowing visualization of redox activity. The reactivity of grain structures in titanium alloys has also been explored using SECM feedback measurements as a function of substrate potential (127), whereas, at higher resolution, CP-AFM has provided insight into the conductivity of passive films that complement SECM measurements (128). The complementarity of SECM and CP-AFM is also well illustrated in studies of other materials, such as dimensionally stable $Ti/TiO_2/Pt$ electrodes (129), wherein two types of active Pt sites were identified and shown to be correlated with the nature of the contact to the underlying substrate.

The SECM tip can be used to initiate local reactions, such as corrosion, and can monitor the consequences via the tip current response and/or topographical analysis of the resulting surface. This approach is evident in studies in which Cl^- was generated by electrolysis of a precursor compound at an SECM tip in order to induce the corrosion of iron (130). SECM tips can also detect the species released or taken up during corrosion via amperometry or ion-selective electrode probes (131).

7.2. Heterogeneous Photochemical Reactions at Semiconductors

In early work, SECM was used to probe electron transfer kinetics for a range of outer-sphere redox couples at n- and p-WSe_2 electrodes in aqueous electrolytes and at n-Si in acetonitrile and methanol (132). These studies surmounted the difficulties and problems inherent in alternative conventional techniques, for example ohmic effects, charging currents, and parallel processes such as corrosion. In subsequent

studies, SECM provided insights into processes at illuminated semiconductor-electrolyte interfaces, exemplified by feedback measurements to probe the photoelectron transfer kinetics for the methyl viologen redox couple ($MV^{2+/+}$) at CdS films (133).

Nanostructured semiconductor films, relevant to applications in photocatalysis and for photovoltaics, have recently been investigated with SECM. In one study, Cl^- was detected with an ion-selective electrode during the photomineralization of chlorophenols (134), and the depletion of O_2 at TiO_2 during photomineralization has also been monitored (135). In both cases, the well-defined mass transport between the UME probe and illuminated surfaces allowed quantitative interpretation of measured fluxes in terms of the underlying kinetics. A time-of-flight SECM technique has been used to measure the diffusion coefficient of redox species in a nanostructured film operated under solar cell conditions (136), whereas the feedback mode has been used to probe the reduction kinetics of photo-oxidized immobilized dye molecules (eosin-Y) by iodide (137). The latter examples illustrate the wide range of processes that can be addressed with SECM.

7.3. Nanostructured Interfaces

The properties of two-dimensional nanoparticle assemblies and nanotube networks have been explored using SECM. The kinetics of hydrogen evolution at gold nanoparticles immobilized on an insulating glass surface were investigated using the SECM feedback mode, in which MV^{2+} was reduced to $MV^{+\cdot}$ at an Hg-Au amalgam UME tip (138). $MV^{+\cdot}$ served as an electron donor in the reduction of protons to hydrogen at the nanoparticle assembly, generating MV^{2+} at the substrate surface that was then fed back to the SECM tip. These feedback current measurements provided quantitative information on H_2 evolution kinetics, which could be interpreted at the single-nanoparticle level.

An important matter in the study of nanoparticle assemblies is the degree of connectivity and the associated lateral conductivity. SECM feedback measurements have proved powerful in monitoring the connectivity of a monolayer of monodisperse thiol-capped silver nanoparticles at the A/W interface via approach curve measurements as a function of surface pressure (53). These experiments involved the deployment of SECM in a Langmuir trough, in an arrangement similar to that discussed in Section 4.2 above for studies of monolayer molecular films. Using the oxidation of ferrocene methanol as the tip redox process, a transition from negative to positive feedback (connected substrate) was observed as the surface pressure was increased. This type of approach has also been used to examine the effect of surface pressure on the conductivity of a polyaniline monolayer (139), in which an insulating-to-conducting transition was observed at a threshold surface pressure.

The conductivity of films on solid supports has also been examined using the SECM feedback mode. Example applications include measuring the conductivity of a monolayer of hexanethiol stabilized gold nanoparticles (140) and polymer-nanoparticle composite films (141, 142). Transient SECM techniques, which involve measuring the current-time response of the SECM tip as a function of a defined

potential-step time program, have been used to provide complementary information on charge injection and lateral charge propagation in ultrathin polymer films (143).

Single-walled carbon nanotubes (SWNTs) are attracting considerable attention for a variety of applications in electroanalysis and electrocatalysis, although there are questions concerning the nature of the active sites and intrinsic electroactivity. SECM feedback measurements have allowed an assessment of electrochemical processes at pristine SWNTs grown on an insulating support without any further processing of the SWNTs (144). One interpretation of these measurements is that SWNT networks may essentially behave as metallic films on typical voltammetric time scales even though the fractional surface coverage of SWNTs is only ~1%.

7.4. Crystal Dissolution, Adsorption, and Desorption

Transient SECM techniques are versatile as a means of introducing a short perturbation to an interfacial system, initially at equilibrium, and measuring the kinetic consequences of the perturbation. In these applications, a UME tip is used to drive desorption processes (56), adsorption processes (145), and dissolution reactions (146) as consequences of an electrochemical process at the tip which changes the local solution composition and thus the equilibrium. The kinetics of the process, initiated electrochemically, is reflected in the SECM current-time response, which can be analyzed using appropriate mass transport models to provide kinetic information. In the case of dissolution, the process naturally leads to a change in surface topography, which can be investigated using complementary techniques. The combination of SECM with AFM, discussed in Section 8.2 below, has provided a means of rapidly assessing dissolution processes in situ at high spatial resolution.

8. HYBRID TECHNIQUES

SECM has been combined with several other techniques to enhance and complement the information available from SECM alone. Considerable effort has gone into developments that provide nonelectrochemical means of monitoring topography, as highlighted in Sections 8.1 and 8.2, and combinations with other techniques (see Section 8.3) have produced multifunctional instruments.

8.1. Shear Force Positioning Methods

The use of shear force positioning opens up the possibility of imaging a sample at constant separation between the tip and surface so that the electrochemical signal is not convoluted by variations in the tip/substrate separation, which may complicate simple SECM experiments in certain applications. However, the implementation of shear force positioning remains nonroutine and rather complex. The UME can be excited to undergo a lateral motion by either a piezoelectric actuator (147) or by attaching the UME to one arm of a tuning fork (97). Both the amplitude and the phase of the tip motion are sensitive to the tip/substrate separation, but it is important to

note that the shear force signal arises from the entire probe end, which usually leads to lower spatial resolution compared to that of the electrochemical signal.

8.2. Scanning Electrochemical–Atomic Force Microscopy

Recent work has seen the integration of UMEs into AFM tips for use in a technique termed SECM-AFM (148). The benefits of SECM-AFM are that one can use the AFM component of the tip for high-resolution topographical imaging or for maintaining a desired tip/substrate separation, whereas the SECM component can be used to electrochemically measure and/or perturb a system. These probes can be used in conjunction with any commercially available AFM instruments. The origins of SECM-AFM can be traced to work in which conventional AFM tips were sputter-coated with a metal so that the entire tip and cantilever could function as an electrode (149). The latter probes have proved beneficial for inducing and monitoring surface reactions such as dissolution (150) and for imaging electroactive surfaces in air (151).

The original high-resolution SECM-AFM probe was produced by coating an etched and flattened microwire with an electrophoretic paint (17, 148). The flattened section provided a flexible cantilever (force sensor), and the coated etched tip served as an electrode. SECM-AFM probes with conical-shaped electrodes of size 10–1000 nm have been fabricated in this way and have found application in reactivity mapping (149) and in studies of transport through membranes (152). This style of probe has also been used to image the conductivity of heterogeneous surfaces, particularly for hard surfaces where thin-film metal-coated probes may be subject to wear (122).

A second method involves coating a silicon nitride tip in a metal, as for integrated electrochemical AFM probes (149), and then insulating the entire probe. The electrode is exposed using a focused ion beam (FIB) (153) to leave a small electrode area. This type of probe has been used to map immobilized enzyme activity and substrate topography (154, 155). Ultrahigh-resolution imaging probes have been produced by attaching bundles of single-walled carbon nanotubes to the tip of a metal-coated AFM tip and using these as a template for the deposition of a metal nanowire (156). The probe is insulated and the end of the nanowire is cut by a FIB to expose a disk-shaped electrode, with a diameter typically in the range of 50–100 nm.

There have been recent advances toward the development of batch fabrication procedures. Using electron beam lithography, it has been possible to produce probes of a reproducible nature from a silicon wafer (157). Ring electrodes integrated into AFM tips have also been fabricated in a batch process (158). This type of methodology offers great promise for the parallel fabrication of many probes with similar characteristics.

8.3. Coupling Scanning Electrochemical Microscopy and Other Methods

In Section 5.5 above we highlight advances in combining SECM with optical techniques. SECM has also been integrated with laser scanning confocal microscopy,

which allows direct visualization of three-dimensional concentration profiles on a rapid time scale and similar length scale to many SECM investigations (96, 159). Studies in this area are at an early stage, but the ability to follow concentration profiles optically, and to follow simultaneously the local electrochemical signal from SECM, is anticipated to provide additional insights into a myriad of interfacial physicochemical processes.

SECM has also been combined with surface-sensitive techniques such as the quartz-crystal microbalance (QCM) (160) and surface plasmon resonance (SPR) (161). These techniques are employed on macroscopic samples, and SECM can be used simultaneously with the QCM or SPR signal to provide local information on associated chemical processes, such as uptake and release from a surface of interest.

DISCLOSURE STATEMENT

The authors are not aware of any biases that might be perceived as affecting the objectivity of this review.

LITERATURE CITED

1. Bard A, Mirkin M, eds. 2001. *Scanning Electrochemical Microscopy*. New York: Marcel Dekker
2. Nagahara L, Tundat T, Lindsay S. 1989. Preparation and characterization of STM tips for electrochemical studies. *Rev. Sci. Instrum.* 60:3128–30
3. Sun P, Zhang Z, Guo J, Shao Y. 2001. Fabrication of nm-sized electrodes and tips for scanning electrochemical microscopy. *Anal. Chem.* 73:5346–51
4. Slevin C, Gray N, Macpherson J, Webb M, Unwin P. 1999. Fabrication and characterization of nm-sized platinum-electrodes for voltammetric analysis and imaging. *Electrochem. Commun.* 1:282–88
5. Zhan W, Bard A. 2006. Scanning electrochemical microscopy. 56. Probing outside and inside single giant liposomes containing $Ru(bpy)_3^{2+}$. *Anal. Chem.* 78:726–33
6. Shao Y, Mirkin M, Fish G, Kokotov S, Palanker D, Lewis A. 1997. Nm-sized electrochemical sensors. *Anal. Chem.* 69:1627–34
7. Katemann B, Schuhmann W. 2002. Fabrication and characterization of needle-type Pt-disk nanoelectrodes. *Electroanalysis* 14:22–28
8. Sun P, Mirkin M. 2006. Kinetics of electron-transfer reactions at nanoelectrodes. *Anal. Chem.* 78:6526–34
9. Sun P, Mirkin M. 2007. Scanning electrochemical microscopy with slightly recessed nanotips. *Anal. Chem.* 79:5809–16
10. Mirkin M, Fan F-R, Bard A. 1992. Scanning electrochemical microscopy. 13. Evaluation of the tip shapes of nm size microelectrodes. *J. Electroanal. Chem.* 328:47–62
11. Mirkin M, Fan F-R, Bard A. 1992. Direct electrochemical measurements inside a 2000-angstrom thick polymer film by scanning electrochemical microscopy. *Science* 257:364–66

12. Fan F-R, Mirkin M, Bard A. 1994. Polymer-films on electrodes. 25. Effect of polymer resistance on the electrochemistry of poly(vinylferrocene): scanning electrochemical microscopic, chronoamperometric, and cyclic voltammetric studies. *J. Phys. Chem.* 98:1475–81
13. Bard A, Fan F-R. 1992. Introductory lecture studies of the liquid-solid interface by scanning-tunneling-microscopy and scanning electrochemical microscopy. *Faraday Discuss. Chem. Soc.* 94:1–22
14. Katemann B, Schulte A, Schuhmann W. 2004. Constant-distance mode scanning electrochemical microscopy. Part II: High-resolution SECM imaging employing Pt nanoelectrodes as miniaturized scanning probes. *Electroanalysis* 16:60–65
15. Baltes N, Thouin L, Amatore C, Heinze J. 2004. Imaging concentration profiles of redox-active species with nanometric amperometric probes: effect of natural convection on transport at microdisk electrodes. *Angew. Chem. Int. Ed.* 43:1431–35
16. Fan F-R, Bard A. 1995. STM on wet insulators: electrochemistry or tunneling? *Science* 270:1849–52
17. Macpherson J, Unwin P. 2001. Noncontact electrochemical imaging with combined scanning electrochemical atomic force microscopy. *Anal. Chem.* 73:550–57
18. Kueng A, Kranz C, Lugstein A, Bertagnolli E, Mizaikoff B. 2003. Integrated AFM-SECM in tapping mode: simultaneous topographical and electrochemical imaging of enzyme activity. *Angew. Chem. Int. Ed.* 42:3238–40
19. Fan F-R, Bard A. 1995. Electrochemical detection of single molecules. *Science* 267:871–74
20. Fan F-R, Kwak J, Bard A. 1996. Single-molecule electrochemistry. *J. Am. Chem. Soc.* 118:9669–75
21. Barker A, Gonsalves M, Macpherson J, Slevin C, Unwin P. 1999. Scanning electrochemical microscopy: beyond the solid/liquid interface. *Anal. Chim. Acta* 385:223–40
22. Mirkin M, Tsionsky M, eds. 2001. Charge transfer at the liquid/liquid interface. In *Scanning Electrochemical Microscopy*, ed. A Bard, M Mirkin, pp. 299–342. New York: Marcel Dekker
23. Wei C, Bard A, Mirkin M. 1995. Scanning electrochemical microscopy. 31. Application of SECM to the study of charge-transfer processes at the liquid-liquid interface. *J. Phys. Chem.* 99:16033–42
24. Shao Y, Mirkin M. 1997. Scanning electrochemical microscopy (SECM) of facilitated ion transfer at the liquid/liquid interface. *J. Electroanal. Chem.* 439:137–43
25. Shao Y, Mirkin M. 1998. Probing ion transfer at the liquid/liquid interface by scanning electrochemical microscopy (SECM). *J. Phys. Chem. B* 102:9915–21
26. Selzer Y, Mandler D. 2000. Probing the coupling of charge-transfer processes across liquid/liquid interfaces by the scanning electrochemical microscope. *J. Phys. Chem. B* 104:4903–10

27. Zhang Z, Yuan Y, Sun P, Su B, Guo J, et al. 2002. Study of electron-transfer reactions across an externally polarized water/1,2-dichloroethane interface by scanning electrochemical microscopy. *J. Phys. Chem. B* 106:6713–17
28. Sun P, Zhang Z, Gao Z, Shao Y. 2002. Probing fast facilitated ion transfer across an externally polarized liquid-liquid interface by scanning electrochemical microscopy. *Angew. Chem. Int. Ed.* 41:3445–48
29. Tsionsky M, Bard A, Mirkin M. 1996. Scanning electrochemical microscopy. 34. Potential dependence of the electron-transfer rate and film formation at the liquid/liquid interface. *J. Phys. Chem.* 100:17881–88
30. Tsionsky M, Bard A, Mirkin M. 1997. Long-range electron-transfer through a lipid monolayer at the liquid/liquid interface. *J. Am. Chem. Soc.* 119:10785–92
31. Ding Z, Quinn B, Bard A. 2001. Kinetics of heterogeneous electron-transfer at liquid/liquid interfaces as studied by SECM. *J. Phys. Chem. B* 105:6367–74
32. Zhang J, Unwin P. 2002. Microelectrochemical measurements of electron transfer rates at the interface between two immiscible electrolyte solutions: Potential dependence of the ferro/ferricyanide-7,7,8,8-tetracyanoquinodimethane (TCNQ)/TCNQ system. *Phys. Chem. Chem. Phys.* 4:3820–27
33. Liu B, Mirkin M. 1999. Potential-independent electron transfer rate at the liquid/liquid interface. *J. Am. Chem. Soc.* 121:8352–55
34. Barker A, Unwin P, Amemiya S, Zhou J, Bard A. 1999. Scanning electrochemistry microscopy (SECM) in the study of electron transfer kinetics at liquid/liquid interfaces: Beyond the constant composition approximation. *J. Phys. Chem. B* 103:7260–69
35. Sun P, Li F, Chen Y, Zhang M, Gao Z, Shao Y. 2003. Observation of the Marcus inverted region of electron transfer reactions at a liquid/liquid interface. *J. Am. Chem. Soc.* 125:9600–1
36. Laforge F, Kakiuchi T, Shigematsu F, Mirkin M. 2004. Comparative study of electron transfer reactions at the ionic liquid/water and organic/water interfaces. *J. Am. Chem. Soc.* 126:15380–81
37. Laforge F, Kakiuchi T, Shigematsu F, Mirkin M. 2006. SECM study of solute partitioning and electron transfer at the ionic liquid/water interface. *Langmuir* 22:10705–10
38. Quinn B, Liljeroth P, Kontturi K. 2002. Interfacial reactivity of monolayer-protected clusters studied by scanning electrochemical microscopy. *J. Am. Chem. Soc.* 124:12915–21
39. Georganopoulou D, Mirkin M, Murray RW. 2004. SECM measurement of the fast electron transfer dynamics between Au-38(1+) nanoparticles and aqueous redox species at a liquid/liquid interface. *Nano Lett.* 4:1763–67
40. Barker A, Unwin P. 2001. Measurement of solute partitioning across liquid/liquid interfaces using scanning electrochemical microscopy–double potential step chronoamperometry (SECM-DPSC): principles, theory, and application to ferrocenium ion transfer across the 1,2-dichloroethane/aqueous interface. *J. Phys. Chem. B* 105:12019–31
41. Zhang J, Strutwolf J, Cannan S, Unwin P. 2003. Combined scanning electrochemical microscopy–Langmuir trough technique for investigating phase

transfer kinetics across liquid/liquid interfaces modified by a molecular monolayer. *Electrochem. Commun.* 5:105–10

42. Liu B, Bard A, Mirkin M, Creager S. 2004. Electron transfer at self-assembled monolayers measured by scanning electrochemical microscopy. *J. Am. Chem. Soc.* 126:1485–92
43. Cannes C, Kanoufi F, Bard A. 2003. Cyclic voltammetry and scanning electrochemical microscopy of ferrocenemethanol at monolayer and bilayer-modified gold electrodes. *J. Electroanal. Chem.* 547:83–91
44. Delville M, Tsionsky M, Bard A. 1998. Scanning electrochemical microscopy studies of electron transfer through monolayers containing conjugated species at the liquid-liquid interface. *Langmuir* 14:2774–79
45. Liu B, Mirkin M. 2002. Electron transfer at liquid/liquid interfaces. The effects of ionic adsorption, electrolyte concentration, and spacer length on the reaction rate. *J. Phys. Chem. B* 106:3933–40
46. Zhang J, Slevin C, Morton C, Scott P, Walton D, Unwin P. 2001. New approach for measuring lateral diffusion in Langmuir monolayers by scanning electrochemical microscopy (SECM): theory and application. *J. Phys. Chem.* 105:11120–30
47. Finklea H. 1996. Electrochemistry of organized monolayers of thiols and related molecules on electrodes. In *Electroanalytical Chemistry*, vol. 19, ed. AJ Bard, H Lund, pp. 109–335. New York: Marcel Dekker
48. Lesia V, Protsailo W, Fawcett R. 2000. Studies of electron transfer through self-assembled monolayers using impedance spectroscopy. *Electrochim. Acta* 45:3497–505
49. Cohen-Atiya M, Nelson A, Mandler D. 2006. Characterization of n-alkanethiol self-assembled monolayers on mercury by impedance and potentiometric measurements. *J. Electroanal. Chem.* 593:227–40
50. Cohen-Atiya M, Mandler D. 2006. Studying electron transfer through alkanethiol self-assembled monolayers on a hanging mercury drop electrode using potentiometric measurements. *Phys. Chem. Chem. Phys.* 8:4405–409
51. Slevin C, Unwin P. 2000. Lateral proton diffusion rates along stearic acid monolayers. *J. Am. Chem. Soc.* 122:2597–602
52. Slevin C, Ryley S, Walton D, Unwin P. 1998. A new approach for measuring the effect of a monolayer on molecular transfer across an air/water interface using scanning electrochemical microscopy. *Langmuir* 14:5331–34
53. Quinn B, Prieto I, Haram S, Bard A. 2001. Electrochemical observation of a metal/insulator transition by scanning electrochemical microscopy. *J. Phys. Chem. B* 105:7474–76
54. Slevin C, Umbers J, Atherton J, Unwin P. 1996. A new approach to the measurement of transfer rates across immiscible liquid/liquid interfaces. *J. Chem. Soc., Faraday Trans.* 92:5177–80
55. Mauzeroll J, Buda M, Bard A, Prieto F, Rueda M. 2002. Detection of Tl(I) transport through a gramicidin-dioleoylphosphatidylcholine monolayer using the substrate generation-tip collection mode of scanning electrochemical microscopy. *Langmuir* 18:9453–61

56. Unwin P, Bard A. 1992. Scanning electrochemical microscopy. 14. Scanning electrochemical microscope induced desorption: a new technique for the measurement of adsorption/desorption kinetics at the solid/liquid interface. *J. Phys. Chem.* 96:5035–45
57. Zhang J, Unwin P. 2002. Proton diffusion at phospholipid assemblies. *J. Am. Chem. Soc.* 124:2379–83
58. Tien H. 1978. *Bilayer Lipid Membranes (BLM): Theory and Practice*. New York: Marcel Dekker
59. Tsionsky M, Zhou J, Amemiya S, Fan F-R, Bard A, Dryfe R. 1999. Scanning electrochemical microscopy. 38. Application of SECM to the study of charge transfer through bilayer lipid membranes. *Anal. Chem.* 71:4300–5
60. Amemiya S, Bard A. 2000. Scanning electrochemical microscopy. 40. Voltammetric ion-selective micropipet electrodes for probing ion transfer at bilayer lipid membranes. *Anal. Chem.* 72:4940–48
61. Lee C, Bard A. 1990. Scanning electrochemical microscopy: application to polymer and thin metal oxide films. *Anal. Chem.* 62:1906–13
62. Lee C, Anson F. 1992. Use of electrochemical microscopy to examine counter ion ejection from Nafion coatings on electrodes. *Anal. Chem.* 64:528–33
63. Arca M, Mirkin M, Bard A. 1995. Polymer films on electrodes. 26. Study of ion transport and electron transfer at polypyrrole films by scanning electrochemical microscopy. *J. Phys. Chem.* 99:5040–50
64. Bath B, White H, Scott E. 2001. Imaging molecular transport across membranes. In *Scanning Electrochemical Microscopy*, ed. A Bard, M Mirkin, pp. 343–96. New York: Marcel Dekker
65. Kueng A, Kranz C, Mizaikoff B. 2005. Imaging of ATP membrane transport with dual micro-disk electrodes and scanning electrochemical microscopy. *Biosens. Bioelectron.* 21:346–53
66. Carano M, Lion N, Abid J, Girault H. 2004. Detection of proteins on poly(vinylidene difluoride) membranes by scanning electrochemical microscopy. *Electrochem. Commun.* 6:1217–21
67. Kallio T, Slevin C, Sundholm G, Holmlund P, Kontturi K. 2003. Proton transport in radiation-grafted membranes for fuel cells as detected by SECM. *Electrochem. Commun.* 5:561–65
68. Uitto O, White H. 2001. Scanning electrochemical microscopy of membrane transport in the reverse imaging mode. *Anal. Chem.* 73:533–39
69. Uitto O, White H, Aoki K. 2002. Diffusive-convective transport into a porous membrane. A comparison of theory and experiment using scanning electrochemical microscopy operated in reverse imaging mode. *Anal. Chem.* 74:4577–82
70. Ervin E, White H, Baker L. 2005. Alternating current impedance imaging of membrane pores using scanning electrochemical microscopy. *Anal. Chem.* 77:5564–69
71. Ervin E, White H, Baker L, Martin C. 2006. Alternating current impedance imaging of high-resistance membrane pores using a scanning electrochemical microscope. Application of membrane electrical shunts to increase measurement sensitivity and image contrast. *Anal. Chem.* 78:6535–41

72. Horrocks B, Schmidtke D, Heller A, Bard A. 1993. Scanning electrochemical microscopy. 24. Enzyme ultramicroelectrodes for the measurement of hydrogen peroxide at surfaces. *Anal. Chem.* 65:3605–14
73. Alpuche-Aviles M, Wipf D. 2001. Impedance feedback control for scanning electrochemical microscopy. *Anal. Chem.* 73:4873–81
74. Katemann B, Inchaispe C, Castro P, Schulte A, Calvo E, Schuhmann W. 2003. Precursor sites for the localized corrosion on lacquered tinplates visualized by means of alternating current scanning electrochemical microscopy. *Electrochim. Acta* 48:1115–21
75. LeSuer R, Fan F-R, Bard A. 2004. Scanning electrochemical microscopy. 52. Bipolar conductance technique at ultramicroelectrodes for resistance measurements. *Anal. Chem.* 76:6894–901
76. Johnson D, Enke C. 1970. Bipolar pulse technique for fast conductance measurements. *Anal. Chem.* 42:329–35
77. Taylor J, LeSuer R, Chambers C, Fan F-R, Bard A, et al. 2005. Experimental techniques for detection of components extracted from model 193 nm immersion lithography photoresists. *Chem. Mater.* 17:4194–203
78. Yasukawa T, Kaya T, Matsue T. 2000. Characterization and imaging of single cells with scanning electrochemical microscopy. *Electroanalysis* 12:653–59
79. Bard A, Li X, Zhan W. 2006. Chemical imaging of living cells by scanning electrochemical microscopy. *Biosens. Bioelectron.* 22:461–72
80. Amemiya S, Guo J, Xiong H, Gross D. 2006. Biological applications of scanning electrochemical microscopy: Chemical imaging of single living cell and beyond. *Anal. Bioanal. Chem.* 386:458–71
81. Edwards M, Martin S, Whitworth A, Macpherson J, Unwin P. 2006. Scanning electrochemical microscopy: principles and applications to biophysical systems. *Physiol. Meas.* 27:R63–R108
82. Yasukawa T, Kondo Y, Uchida I, Matsue T. 1998. Imaging of cellular activity of single cultured cells by scanning electrochemical microscopy. *Chem. Lett.* 8:767–68
83. Shiku H, Shiraishi T, Ohya H, Matsue T, Abe H, et al. 2001. Oxygen consumption of single bovine embryos probed by scanning electrochemical microscopy. *Anal. Chem.* 73:3751–58
84. Kaya T, Torisawa Y, Oyamatsu D, Nishizawa M, Matsue T. 2003. Monitoring the cellular activity of a cultured single cell by scanning electrochemical microscopy (SECM). A comparison with fluorescence viability monitoring. *Biosens. Bioelectron.* 18:1379–83
85. Zhan D, Li X, Zhan W, Fan F-R, Bard A. 2007. Scanning electrochemical microscopy. 58. Application of a micropipet-supported ITIES tip to detect Ag^+ and study its effect on fibroblast cells. *Anal. Chem.* 79:5225–31
86. Liu B, Rotenberg S, Mirkin M. 2000. Scanning electrochemical microscopy of living cells: Different redox activities of nonmetastatic and metastatic human breast cells. *Proc. Natl. Acad. Sci. USA* 97:9855–60
87. Liu B, Rotenberg S, Mirkin M. 2002. Scanning electrochemical microscopy of living cells. 4. Mechanistic study of charge transfer reactions in human breast cells. *Anal. Chem.* 74:6340–48

88. Rotenberg S, Mirkin M. 2004. Scanning electrochemical microscopy: detection of human breast cancer cells by redox environment. *J. Mammary Gland Biol.* 9:375–82
89. Feng W, Rotenberg S, Mirkin M. 2003. Scanning electrochemical microscopy of living cells. 5. Imaging of fields of normal and metastatic human breast cells. *Anal. Chem.* 75:4148–54
90. Mauzeroll J, Bard A. 2004. Scanning electrochemical microscopy of menadione-glutathione conjugate export from yeast cells. *Proc. Natl. Acad. Sci. USA* 101:7862–67
91. Mauzeroll J, Bard A, Owhadian O, Monks T. 2004. Menadione metabolism to thiodione in hepatoblastoma by scanning electrochemical microscopy. *Proc. Natl. Acad. Sci. USA* 101:17582–87
92. Guo J, Amemiya S. 2005. Permeability of the nuclear envelope at isolated *Xenopus* oocyte nuclei studied by scanning electrochemical microscopy. *Anal. Chem.* 77:2147–56
93. Hengstenberg A, Blöchl A, Dietzel I, Schuhmann W. 2001. Spatially resolved detection of neurotransmitter secretion from individual cells by means of scanning electrochemical microscopy. *Angew. Chem. Int. Ed.* 40:905–908
94. Takahashi Y, Hirano Y, Yasukawa T, Shiku H, Yamada H, Matsue T. 2006. Topographic, electrochemical, and optical images captured using standing approach mode scanning electrochemical/optical microscopy. *Langmuir* 22:10299–306
95. Kurulugama R, Wipf D, Takacs S, Pongmayteegul S, Garris P, Baur J. 2005. Scanning electrochemical microscopy of model neurons: constant distance imaging. *Anal. Chem.* 77:1111–17
96. Boldt F-M, Heinze J, Diez M, Petersen J, Börsch M. 2004. Real-time pH microscopy down to the molecular level by combined scanning electrochemical microscopy/single-molecule fluorescence spectroscopy. *Anal. Chem.* 76:3473–81
97. Lee Y, Ding Z, Bard A. 2002. Combined scanning electrochemical/optical microscopy with shear force and current feedback. *Anal. Chem.* 74:3634–43
98. Zhao X, Petersen N, Ding Z. 2007. Comparison study of live cells by atomic force microscopy, confocal microscopy, and scanning electrochemical microscopy. *Can. J. Chem.* 85:175–83
99. Zoski C, Simjee N, Guenat O, Koudelka-Hep M. 2004. Addressable microelectrode arrays: Characterization by imaging with scanning electrochemical microscopy. *Anal. Chem.* 76:62–72
100. Jayaraman S, Hillier A. 2003. Screening the reactivity of Pt_xRu_y and $Pt_xRu_yMo_z$ catalysts toward the hydrogen oxidation reaction with the scanning electrochemical microscope. *J. Phys. Chem. B* 107:5221–30
101. Shah B, Hillier A. 2000. Imaging the reactivity of electro-oxidation catalysts with the scanning electrochemical microscope. *J. Electrochem. Soc.* 147:3043–48
102. Jayaraman S, Hillier A. 2004. Construction and reactivity screening of a surface composition gradient for combinatorial discovery of electro-oxidation catalysts. *J. Comb. Chem.* 6:27–31

103. Jayaraman S, Hillier A. 2001. Construction and reactivity mapping of a platinum catalyst gradient using the scanning electrochemical microscope. *Langmuir* 17:7857–64
104. Kucernak A, Chowdhury P, Wilde C, Kelsall G, Zhu Y, Williams D. 2000. Scanning electrochemical microscopy of a fuel-cell electrocatalyst deposited onto highly oriented pyrolytic-graphite. *Electrochim. Acta* 45:4483–91
105. Fernández J, Raghuveer V, Manthiram A, Bard A. 2005. Pd-Ti and Pd-Co-Au electrocatalysts as a replacement for platinum for oxygen reduction in proton exchange membrane fuel cells. *J. Am. Chem. Soc.* 127:13100–1
106. Fernández J, Walsh D, Bard A. 2004. Thermodynamic guidelines for the design of bimetallic catalysts for oxygen electroreduction and rapid screening by scanning electrochemical microscopy. M-Co (M: Pd, Ag, Au). *J. Am. Chem. Soc.* 127:357–65
107. Walsh D, Fernández J, Bard A. 2006. Rapid screening of bimetallic electrocatalysts for oxygen reduction in acidic media by scanning electrochemical microscopy. *J. Electrochem. Soc.* 153:E99–E103
108. Weng Y, Fan F-R, Bard A. 2005. Combinatorial biomimetics. Optimization of a composition of copper(II) poly-L-histidine complex as an electrocatalyst for O_2 reduction by scanning electrochemical microscopy. *J. Am. Chem. Soc.* 127:17576–77
109. Fernández J, Mano N, Heller A, Bard A. 2004. Optimization of "wired" enzyme O_2-electroreduction catalyst compositions by scanning electrochemical microscopy. *Angew. Chem. Int. Ed.* 43:6355–57
110. Black M, Cooper J, McGinn P. 2005. Scanning electrochemical microscope characterization of thin film combinatorial libraries for fuel cell electrode applications. *Meas. Sci. Technol.* 16:174–82
111. Zhou J, Zu Y, Bard A. 2000. Scanning electrochemical microscopy. 39. The proton/hydrogen mediator system and its application to the study of the electrocatalysis of hydrogen oxidation. *J. Electroanal. Chem.* 491:22–29
112. Jambunathan K, Shah B, Hudson J, Hillier A. 2000. Scanning electrochemical microscopy of hydrogen electro-oxidation. Rate constant measurements and carbon monoxide poisoning on platinum. *J. Electroanal. Chem.* 500:279–89
113. Liu B, Bard A. 2002. Scanning electrochemical microscopy. 45. Study of the kinetics of oxygen reduction on platinum with potential programming of the tip. *J. Phys. Chem. B* 106:12801–806
114. Zoski C. 2003. Investigation of hydrogen electrocatalysis at polycrystalline noble metal electrodes by scanning electrochemical microscopy. *J. Phys. Chem. B* 107:6401–5
115. Fernández J, Bard A. 2004. Scanning electrochemical microscopy. 50. Kinetic study of electrode reactions by the tip generation-substrate collection mode. *Anal. Chem.* 76:2281–89
116. Lu G, Cooper J, McGinn P. 2007. SECM imaging of electrocatalytic activity for oxygen reduction reaction on thin film materials. *Electrochim. Acta* 52:5172–81
117. Zoski C, Aguilar J, Bard A. 2003. Scanning electrochemical microscopy. 46. Shielding effects on reversible and quasireversible reactions. *Anal. Chem.* 75:2959–66

118. Zoski C, Luman C, Fernández J, Bard A. 2007. Scanning electrochemical microscopy. 57. SECM tip voltammetry at different substrate potentials under quasi-steady-state and steady-state conditions. *Anal. Chem.* 79:4957–66
119. Eckhard K, Chen X, Turcu F, Schuhmann W. 2006. Redox-competition mode of scanning electrochemical microscopy (SECM) for visualisation of local catalytic activity. *Phys. Chem. Chem. Phys.* 8:5359–65
120. Karnicka K, Eckhard K, Guschin D, Stoica L, Kulesza P, Schuhmann W. 2007. Visualisation of the local bio-electrocatalytic activity in biofuel cell cathodes by means of redox competition scanning electrochemical microscopy (RC-SECM). *Electrochem. Commun.* 9:1998–2002
121. Holt K, Bard A, Show Y, Swain G. 2004. Scanning electrochemical microscopy and conductive probe atomic force microscopy studies of hydrogen-terminated boron-doped diamond electrodes with different doping levels. *J. Phys. Chem. B* 108:15117–27
122. Wilson N, Clewes S, Newton M, Unwin P, Macpherson J. 2006. Impact of grain-dependent boron uptake on the electrochemical and electrical properties of boron doped polycrystalline diamond electrodes. *J. Phys. Chem. B* 110:5639–46
123. Szunerits S, Mermoux M, Crisci A, Marcus B, Bouvier P, et al. 2006. Raman imaging and Kelvin probe microscopy for the examination of the heterogeneity of doping in polycrystalline boron-doped diamond electrodes. *J. Phys. Chem. B* 110:23888–97
124. Basame S, White H. 1998. Scanning electrochemical microscopy: measurement of the current density at microscopic redox-active sites on titanium. *J. Phys. Chem. B* 102:9812–19
125. Basame S, White H. 1999. Chemically-selective and spatially-localized redox activity at Ta/Ta_2O_5 electrodes. *Langmuir* 15:819–25
126. Serebrennikova I, White H. 2001. Scanning electrochemical microscopy of electroactive defect sites in the native oxide film on aluminium. *Electrochem. Solid State Lett.* 4:B4–B6
127. Zhu R, Nowierski C, Ding Z, Noel J, Shoesmith D. 2007. Insights into grain structures and their reactivity on grade-2 Ti alloy surfaces by scanning electrochemical microscopy. *Chem. Mater.* 19:2533–43
128. Boxley C, White H, Gardner C, Macpherson J. 2003. Nanoscale imaging of the electronic conductivity of the native oxide film on titanium using conducting atomic force microscopy. *J. Phys. Chem. B* 107:9677–80
129. Macpherson J, de Mussy J, Delplancke J. 2002. High-resolution electrochemical, electrical, and structural characterization of a dimensionally stable Ti/TiO_2/Pt electrode. *J. Electrochem. Soc.* 149:B306–B313
130. Still J, Wipf D. 1997. Breakdown of the iron passive layer by use of the scanning electrochemical microscope. *J. Electrochem. Soc.* 144:2657–65
131. Gray N, Unwin P. 2000. Simple procedure for the fabrication of silver/silver chloride potentiometric electrodes with micrometre and smaller dimensions: application to scanning electrochemical microscopy. *Analyst* 125:889–93

132. Horrocks B, Mirkin M, Bard A. 1994. Scanning electrochemical microscopy. 25. Application to the kinetics of heterogeneous electron transfer at semiconductor (WSe_2 and Si) electrodes. *J. Phys. Chem.* 98:9106–14
133. Haram S, Bard A. 2001. Scanning electrochemical microscopy. 42. Studies of the kinetics and photoelectrochemistry of thin film CdS/electrolyte interfaces. *J. Phys. Chem. B* 105:8192–95
134. Fonseca S, Barker A, Ahmed S, Kemp T, Unwin P. 2004. Scanning electrochemical microscopy investigation of the photodegradation kinetics of 4-chlorophenol sensitised by TiO_2 films. *Phys. Chem. Chem. Phys.* 6:5218–24
135. Fonseca S, Barker A, Ahmed S, Kemp T, Unwin P. 2003. Direct observation of oxygen depletion and product formation during photocatalysis at a TiO_2 surface using scanning electrochemical microscopy. *Chem. Comm.* 1002–1003
136. Bozic B, Figgemeier E. 2006. Scanning electrochemical microscopy under illumination: an elegant tool to directly determine the mobility of charge carriers within dye-sensitized nanostructured semiconductors. *Chem. Comm.* 2268–70
137. Shen Y, Nonomura K, Schlettwein D, Zhao C, Wittstock G. 2006. Photoelectrochemical kinetics of eosin Y-sensitized zinc oxide films investigated by scanning electrochemical microscopy. *Chem. Eur. J.* 12:5832–39
138. Zhang J, Lahtinen R, Kontturi K, Unwin P, Schiffrin D. 2001. Electron transfer reactions at gold nanoparticles. *Chem. Comm.* 1818–19
139. Zhang J, Barker A, Mandler D, Unwin P. 2003. Effect of surface pressure on the insulator to metal transition of a Langmuir polyaniline monolayer. *J. Am. Chem. Soc.* 125:9312–13
140. Liljeroth P, Quinn B, Ruiz V, Kontturi K. 2003. Charge injection and lateral conductivity in monolayers of metallic nanoparticles. *Chem. Comm.* 1570–71
141. Ruiz V, Liljeroth P, Quinn B, Kontturi K. 2003. Probing conductivity of polyelectrolyte/nanoparticle composite films by scanning electrochemical microscopy. *Nano Lett.* 3:1459–62
142. Ruiz V, Nicholson P, Jollands S, Thomas P, Macpherson J, Unwin P. 2005. Molecular ordering and 2D conductivity in ultrathin poly(3-hexylthiophene)/gold nanoparticle composite films. *J. Phys. Chem. B* 109:19335–44
143. O'Mullane A, Macpherson J, Unwin P, Cervera-Montesinos J, Manzanares J, et al. 2004. Measurement of lateral charge propagation in [Os(bpy)(2)(PVP)(n)Cl]Cl thin films: a scanning electrochemical microscopy approach. *J. Phys. Chem. B* 108:7219–27
144. Wilson N, Guille M, Dumitrescu I, Fernandez V, Rudd N, et al. 2006. Assessment of the electrochemical behavior of two-dimensional networks of single-walled carbon nanotubes. *Anal. Chem.* 78:7006–15
145. Burt D, Cervera J, Mandler D, Macpherson J, Manzanares J, Unwin P. 2005. Scanning electrochemical microscopy as a probe of Ag^+ binding kinetics at Langmuir phospholipid monolayers. *Phys. Chem. Chem. Phys.* 7:2955–64
146. Macpherson J, Unwin P. 1994. A novel approach to the study of dissolution kinetics using the scanning electrochemical microscope: theory and application to copper sulfate pentahydrate dissolution in aqueous sulfuric acid solutions. *J. Phys. Chem.* 98:1704–13

147. Ludwig M, Kranz C, Schuhmann W, Gaub H. 1995. Topography feedback mechanism for the scanning electrochemical microscope based on hydrodynamic forces between the tip and sample. *Rev. Sci. Instrum.* 66:2857–60
148. Macpherson J, Unwin P. 2000. Combined scanning electrochemical-atomic force microscopy. *Anal. Chem.* 72:276–85
149. Macpherson J, Unwin P, Hillier A, Bard A. 1996. In-situ imaging of ionic crystal dissolution using an integrated electrochemical/AFM probe. *J. Am. Chem. Soc.* 118:6445–52
150. Jones C, Unwin P, Macpherson J. 2003. In situ observation of the surface processes involved in dissolution from the cleavage surface of calcite in aqueous solution using combined scanning electrochemical-atomic force microscopy (SECM-AFM). *Chem. Phys. Chem.* 4:139–46
151. Macpherson J, Jones C, Barker A, Unwin P. 2002. Electrochemical imaging of diffusion through single nanoscale pores. *Anal. Chem.* 74:1841–48
152. Gardner C, Unwin P, Macpherson J. 2005. Correlation of membrane structure and transport activity using combined scanning electrochemical-atomic force microscopy. *Electrochem. Commun.* 7:612–18
153. Kranz C, Friedbacher G, Mizaikoff B. 2001. Integrating an ultramicroelectrode in an AFM cantilever: combined technology for enhanced information. *Anal. Chem.* 73:2491–500
154. Kranz C, Kueng A, Lugstein A, Bertagnolli E, Mizaikoff B. 2004. Mapping of enzyme activity by detection of enzymatic products during AFM imaging with integrated SECM-AFM probes. *Ultramicroscopy* 100:127–34
155. Kueng A, Kranz C, Lugstein A, Bertagnolli E, Mizaikoff B. 2005. AFM-tip-integrated amperometric microbiosensors: high-resolution imaging of membrane transport. *Angew. Chem. Int. Ed.* 44:3419–22
156. Burt D, Wilson N, Weaver J, Dobson P, Macpherson J. 2005. Nanowire probes for high resolution combined scanning electrochemical microscopy: atomic force microscopy. *Nano Lett.* 5:639–43
157. Dobson P, Weaver J, Holder M, Unwin P, Macpherson J. 2005. Characterization of batch-microfabricated scanning electrochemical–atomic force microscopy probes. *Anal. Chem.* 77:424–34
158. Shin H, Hesketh P, Mizaikoff B, Kranz C. 2007. Batch fabrication of atomic force microscopy probes with recessed integrated ring microelectrodes at a wafer level. *Anal. Chem.* 79:4769–77
159. Rudd N, Cannan S, Bitziou E, Ciani L, Whitworth A, Unwin P. 2005. Fluorescence confocal laser scanning microscopy as a probe of pH gradients in electrode reactions and surface activity. *Anal. Chem.* 77:6205–17
160. Gollas B, Bartlett P, Denuault G. 2000. An instrument for simultaneous EQCM impedance and SECM measurements. *Anal. Chem.* 72:349–56
161. Xiang J, Guo J, Zhou F. 2006. Scanning electrochemical microscopy combined with surface plasmon resonance: studies of localized film thickness variations and molecular conformation changes. *Anal. Chem.* 78:1418–24

Annual Review of Analytical Chemistry

Volume 1, 2008

Contents